JEM Journal of Experimental Medicine

ARTICLE

Fyn kinase regulates misfolded α-synuclein uptake and NLRP3 inflammasome activation in microglia

Nikhil Panicker[1,2,3], Souvarish Sarkar[1], Dilshan S. Harischandra[1], Matthew Neal[1], Tae-In Kam[2,3], Huajun Jin[1], Hariharan Saminathan[1], Monica Langley[1], Adhithiya Charli[1], Manikandan Samidurai[1], Dharmin Rokad[1], Shivani Ghaisas[1], Olga Pletnikova[7], Valina L. Dawson[2,3,4,5], Ted M. Dawson[2,3,4,6], Vellareddy Anantharam[1], Anumantha G. Kanthasamy[1], and Arthi Kanthasamy[1]

Persistent microglia-mediated neuroinflammation is a major pathophysiological contributor to the progression of Parkinson's disease (PD), but the cell-signaling mechanisms governing chronic neuroinflammation are not well understood. Here, we show that Fyn kinase, in conjunction with the class B scavenger receptor CD36, regulates the microglial uptake of aggregated human α-synuclein (αSyn), which is the major component of PD-associated Lewy bodies. αSyn can effectively mediate LPS-independent priming and activation of the microglial NLRP3 inflammasome. Fyn kinase regulates both of these processes; it mediates PKCδ-dependent NF-κB–p65 nuclear translocation, leading to inflammasome priming, and facilitates αSyn import into microglia, contributing to the generation of mitochondrial reactive oxygen species and consequently to inflammasome activation. In vivo experiments using A53T and viral-αSyn overexpression mouse models as well as human PD neuropathological results further confirm the role of Fyn in NLRP3 inflammasome activation. Collectively, our study identifies a novel Fyn-mediated signaling mechanism that amplifies neuroinflammation in PD.

Introduction

Parkinson's disease (PD) is a neurodegenerative movement disorder characterized by the death of dopaminergic neurons within the nigrostriatal tract. Sterile inflammation mediated primarily by resident brain microglia has gained momentum as both an important mediator of the neuron loss contributing to the progressive nature of PD and an attractive drug target for neurodegenerative disease therapy (Imamura et al., 2003; Block et al., 2007; Glass et al., 2010; Tansey and Goldberg, 2010).

Inflammasomes are large, multimeric protein complexes comprising a cytosolic pattern-recognition receptor, the adaptor protein apoptosis-associated Speck-like protein containing a caspase recruitment domain (ASC), and caspase-1 (Casp-1; Lamkanfi and Dixit, 2014). Their assembly is triggered by a variety of stimuli and culminates in the activation of Casp-1, which then cleaves pro–IL-1β to IL-1β (Latz et al., 2013; Walsh et al., 2014). The Nod-like receptor protein 3 (NLRP3) inflammasome is the best-studied inflammasome and has a two-step activation mechanism: "priming," which entails induction of pro–IL-1β and NLRP3, and "activation," wherein a functional inflammasome complex is assembled following uptake of a pathogen or danger-associated molecular pattern. This is hypothesized to serve as a checkpoint to prevent unabated release of IL-1β. Increased IL-1β and cleaved Casp-1 levels have been demonstrated in PD patient tissues, but this was shown before inflammasome-mediated IL-1β processing was demonstrated (Mogi et al., 1996, 2000). The pathology of various other diseases, including Alzheimer's disease (AD; Heneka et al., 2013), diabetes (Lee et al., 2013), and atherosclerosis (Duewell et al., 2010; Sheedy et al., 2013), has been linked to hyperactivation of the NLRP3 inflammasome. In peripheral immune cells, ASC specks released from inflammasome-activated cells can propagate inflammasome activation in a prionic manner (Baroja-Mazo et al., 2014). Recently, microglia-released ASC specks were found to cross-seed amyloid-β, thereby enhancing AD pathology (Venegas et al., 2017).

α-synuclein (αSyn) is a presynaptic protein whose dysfunction is intimately associated with idiopathic and genetically inherited PD. Mutations of the *SNCA* gene cause autosomal dominant PD (Polymeropoulos et al., 1997; Krüger et al., 1998; Zarranz et al., 2004; Appel-Cresswell et al., 2013; Lesage et al.,

[1]Parkinson Disorders Research Program, Iowa Center for Advanced Neurotoxicology, Department of Biomedical Sciences, Iowa State University, Ames, IA; [2]Neuroregeneration and Stem Cell Programs, Institute for Cell Engineering, Johns Hopkins University School of Medicine, Baltimore, MD; [3]Department of Neurology, Johns Hopkins University School of Medicine, Baltimore, MD; [4]Solomon H. Snyder Department of Neuroscience, Johns Hopkins University School of Medicine, Baltimore, MD; [5]Department of Physiology, Johns Hopkins University School of Medicine, Baltimore, MD; [6]Department of Pharmacology and Molecular Sciences, Johns Hopkins University School of Medicine, Baltimore, MD; [7]Department of Pathology, Johns Hopkins University School of Medicine, Baltimore, MD.

Correspondence to Anumantha Kanthasamy: akanthas@iastate.edu; Arthi Kanthasamy: arthik@iastate.edu.

2013; Pasanen et al., 2014; Allen Reish and Standaert, 2015). Misfolded αSyn is also the major component of PD-associated Lewy bodies, the neuropathological hallmark of PD. αSyn species can transmit from neuron to neuron via self-amplification in vivo, propagating pathology and cell death in a prionic manner (Luk et al., 2012). This transmission is mediated by lymphocyte-activation gene 3 (Mao et al., 2016). The action of αSyn on nonneuronal cells is an active area of investigation; in patients with multiple system atrophy, αSyn accumulates in oligodendrocytes as glial cytoplasmic inclusions (Tu et al., 1998) and can seed endogenous αSyn aggregation with even greater potency than neuronal αSyn (Peng et al., 2018).

αSyn uptake in neurons causes impairment in mitochondrial function (Devi et al., 2008; Luth et al., 2014; Reeve et al., 2015). Dysfunctional mitochondria release excessive amounts of mitochondrial reactive oxygen species (mitoROS), which are necessary and sufficient to activate the NLRP3 inflammasome in macrophages and microglia (Zhou et al., 2011; Sarkar et al., 2017). Although αSyn is known to elicit the production of IL-1β in monocytes and microglia (Codolo et al., 2013; Gustot et al., 2015. Lee et al., 2010; Boza-Serrano et al., 2014; Daniele et al., 2015; Gordon et al., 2018), the inceptive signaling mechanisms that regulate microglial NLRP3 inflammasome assembly have yet to be established. In this study, we demonstrate that Fyn kinase intrinsically regulates both αSyn-mediated priming as well as activation of the microglial NLRP3 inflammasome.

Fyn is a nonreceptor Src family tyrosine kinase known to mediate proinflammatory signaling in T cells, mast cells, natural killer cells, and bone marrow–derived macrophages (BMDMs) in response to diverse activating agents (Moore et al., 2002; Palacios and Weiss, 2004; Gomez et al., 2005; Stuart et al., 2007). In the central nervous system, Fyn mediates amyloid-β–induced apoptosis in cortical neurons (Lambert et al., 1998), and contributes to astrocytic migration (Dey et al., 2008) and the differentiation of oligodendrocytes (Sperber et al., 2001). Very recently, the *FYN* gene was identified in a genome-wide association study (GWAS) as a novel PD risk locus (Nalls et al., 2018 *Preprint*). We demonstrated Fyn's role in inflammogen-mediated proinflammatory signaling in microglia via tyrosine phosphorylation of PKCδ (Panicker et al., 2015). To the best of our knowledge, no study exists on the role that Fyn plays in the activation of the NLRP3 inflammasome in any cell type. Although PKCδ has been shown to play a crucial role in activating the NLRC4 inflammasome via S533 phosphorylation activation (Qu et al., 2012), the current study is also the first to characterize its role in NLRP3 inflammasome activation.

Results

Fyn and CD36 mediate αSyn uptake in microglia

We purified human recombinant αSyn (Fig. S1). αSyn aggregation and protein fibril characterization was performed as previously described (Zhang et al., 2005; Sarkar et al., 2018). αSyn stimulation of primary murine microglia rapidly induced the active loop phosphorylation of Fyn (Fig. 1, A and B). We used the p-Y416 Src family kinase (SFK) antibody to blot for activated Fyn. Since this antibody recognizes all active SFKs, we verified that αSyn did not induce any discernible p-Y416 Src phosphorylation in Fyn$^{-/-}$ microglia (Fig. 1 A).

To demonstrate the activation of Fyn in a well-characterized in vivo αSyn mouse model, we used the adeno-associated virus overexpressing αSyn (AAV-αSyn) model, wherein viral constructs coding for human αSyn or GFP (as a control) are injected into the substantia nigra pars compacta (SNpc) of mice. 30 d after injection, brains from AAV-αSyn–injected (the AAV-SYN group) and adeno-associated virus overexpressing GFP (AAV-GFP) mice were extracted, sectioned, and stained for Iba-1 and p-Y416 SFK. Significantly increased p-Y416 SFK levels within Iba-1–positive microglia were observed in the AAV-SYN group when compared with the AAV-GFP group (Fig. 1 C), indicating that microglial Fyn was activated early in this in vivo PD model.

Immunoprecipitation of CD36 and TLR2 in control and αSyn-stimulated WT primary microglia showed that both receptors interacted with αSyn, but only CD36 interacted with Fyn upon αSyn treatment (Fig. 1 D). Next, we transfected human embryo kidney (HEK) cells with FLAG-tagged human CD36. These cells were then treated with αSyn aggregates for 15, 30, 45, and 60 min. CD36 was immunoprecipitated using a monoclonal FLAG antibody. Immunoblot analysis revealed transient interaction between CD36 and αSyn 15 and 30 min after treatment (Fig. 1 E). αSyn-mediated p-Y416 SFK activation was significantly attenuated in CD36$^{-/-}$ BMDMs (Fig. 1 F), showing that Fyn was activated following CD36 engagement of αSyn.

We next tested whether CD36 and Fyn play a role in the uptake of αSyn. Aggregated αSyn was first added to WT and Fyn$^{-/-}$ microglia as well as WT and CD36$^{-/-}$ BMDMs for various time points. Immunoblots of whole-cell lysates from αSyn-treated Fyn$^{-/-}$ microglia or CD36$^{-/-}$ BMDMs displayed significantly attenuated αSyn uptake in these cells (Fig. 1, G and H). To verify this, immunocytochemistry (ICC) experiments were performed. αSyn-treated WT and Fyn$^{-/-}$ microglia were triple washed with PBS and then fixed and stained for microglial uptake of human αSyn, which was visualized as intracellular puncta (Fig. 1, I and J). The number of puncta per cell was quantified. Fyn$^{-/-}$ microglia display reduced uptake of human αSyn. To confirm these findings, we transfected primary microglia with FLAG-tagged WT and activation loop mutant Fyn (Y417A Fyn), following which the cells were treated with aggregated αSyn for 15, 30, and 45 min (Fig. 1 K). Whole-cell lysates were probed for FLAG and p-Y416 SFK antibodies. WT Fyn-FLAG-transfected cells demonstrated a rapid induction of p-Y416 SFK levels, which was abolished in the Y417A Fyn-FLAG-transfected groups. The import of αSyn was significantly attenuated in the cells transfected with the activation loop mutant Fyn, indicating that Fyn activity was required for αSyn import into microglia.

Microglial Fyn activation in human PD brain

Recently, the *FYN* gene was identified as a novel PD risk locus via GWAS (Nalls et al., 2018 *Preprint*). Analysis of nigral lysates from AAV-GFP and AAV-SYN (SNpc-injected) mice showed a significant induction of Fyn and p-Y416 SFK levels (Fig. 2 A). Immunohistochemistry (IHC) of nigral sections revealed increased

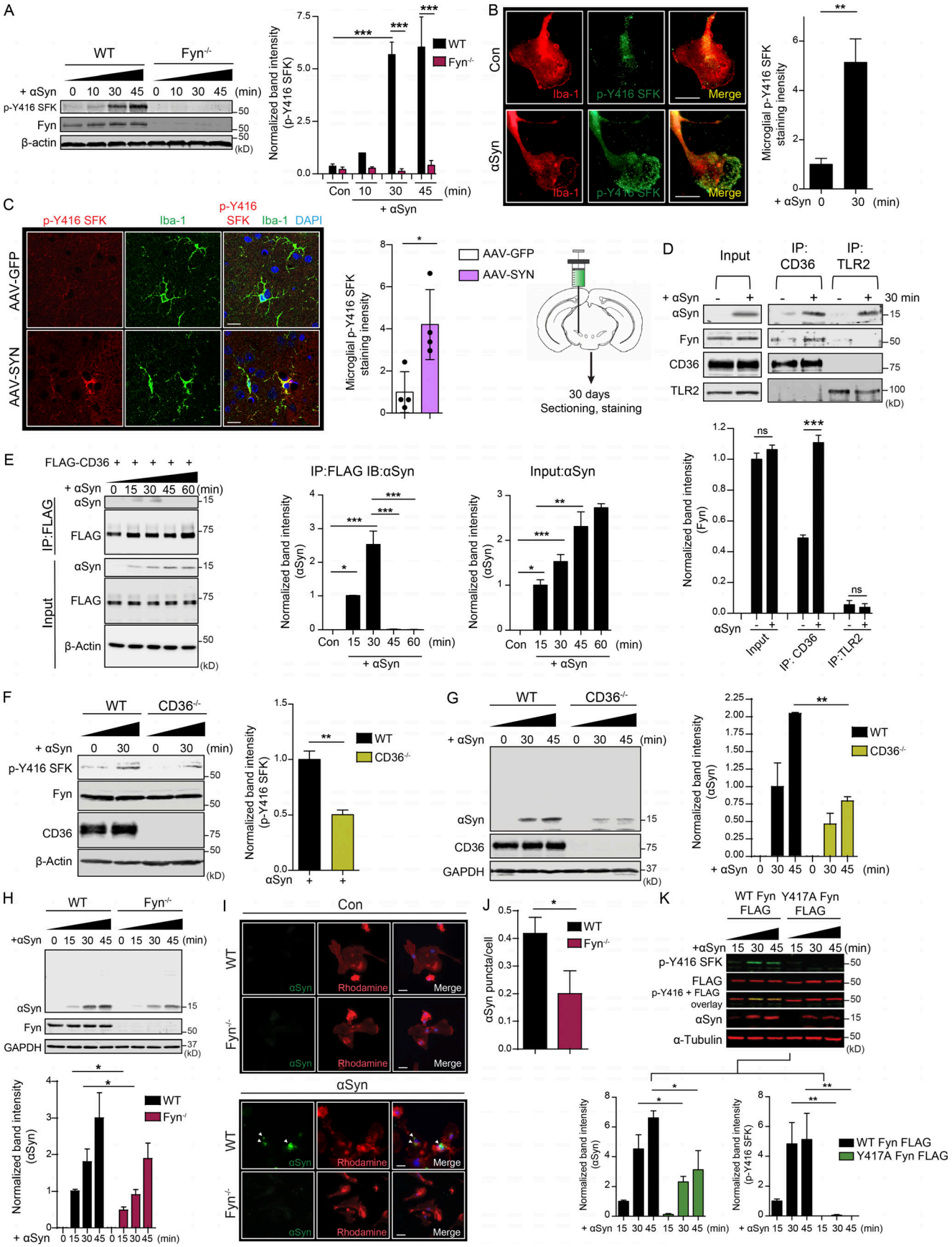

Figure 1. **Fyn and CD36 contribute to aggregated αSyn uptake into microglia**. **(A)** Immunoblot analysis of aggregated αSyn-treated WT and Fyn$^{-/-}$ microglial lysates reveals a rapid induction of SFK activity in WT, but not Fyn$^{-/-}$, microglia. Error bars represent mean ± SEM. One-way ANOVA followed by Tukey's post hoc test (n = 3). Con, control. **(B)** ICC reveals rapid increase in p-Y416 SFK levels in αSyn-treated Iba-1–positive WT microglial cells. Scale bars, 15 µm. Error bars represent mean ± SEM. Unpaired two-tailed t test (n = 4). **(C)** IHC analysis to show microglial Fyn activation in the AAV-SYN model at 30 d. Schematic of AAV injection on the side. Scale bars, 15 µm. Error bars represent mean ± SEM. Unpaired two-tailed t test (n = 4 mice per group). **(D)** Upon its application to microglial cells, αSyn associates with TLR2 and CD36, as evidenced by coIP analysis. Upon αSyn treatment, Fyn associates with CD36, but not TLR2. Error bars represent mean ± SEM. One-way ANOVA followed by Tukey's post hoc test (n = 3). IP, immunoprecipitation. **(E)** Immunoprecipitation of FLAG-tagged human CD36 in αSyn-treated HEK cells shows a transient interaction of CD36 and αSyn. Error bars represent mean ± SEM. One-way ANOVA followed by Tukey's post hoc test (n = 3). IB, immunoblotting. **(F)** Immunoblot for p-Y416 SFK reveals that Fyn activation occurs downstream of CD36. Error bars represent mean ± SEM. Unpaired two-tailed t test (n = 3). **(G)** Immunoblot analysis showing diminished αSyn uptake by CD36$^{-/-}$ BMDMs. Error bars represent mean ± SEM. One-way ANOVA followed by Tukey's post hoc test (n = 3). **(H)** Immunoblot analysis also reveals that reduced αSyn was taken up by Fyn$^{-/-}$ microglia. Error bars represent mean ± SEM. One-way ANOVA followed by Tukey's post hoc test (n = 5). **(I and J)** ICC for human αSyn revealed diminished uptake of the protein in Fyn-deficient microglia. Error bars represent mean ± SEM. Unpaired two-tailed t test (n = 5). Scale bars, 15 µm. **(K)** Whole-cell lysate analysis from αSyn-treated, WT-transfected, and activation loop–deficient (Y417A) Fyn-FLAG–transfected cells showed diminished αSyn uptake in inactive Fyn mutant–expressing cells. Error bars represent mean ± SEM. One-way ANOVA followed by Tukey's post hoc test (n = 3). Asterisks indicate the level of statistical significance: ns, not significant; *, P ≤ 0.05; **, P ≤ 0.01; ***, P ≤ 0.001.

Fyn expression within Iba-1–positive microglia in the AAV-SYN group (Fig. 2 B). It is worth noting that at this time point (45 d after injection), the SNpc region of AAV-SYN mice shows significant microgliosis, as evidenced by the dramatic shift in microglial morphology from ramified to amoeboid. Following this, analysis of ventral midbrain lysates from PD patients and age-matched controls showed significant induction of Fyn expression and activation (Fig. 2 C). IHC of age-matched and PD brain sections revealed increased microgliosis and significantly increased Fyn expression and activation within microglia under PD conditions (Fig. 2, D and E). Details of the postmortem PD and control tissues are provided in Table S1.

αSyn uptake induces mitochondrial dysfunction and mitoROS generation in microglia, leading to NLRP3 inflammasome activation

αSyn causes impairment of mitochondrial function in neurons (Devi et al., 2008; Grassi et al., 2018). To quantify αSyn-induced mitoROS generation in microglia, we used MitoSOX dye. Aggregated αSyn treatment induced progressively increasing

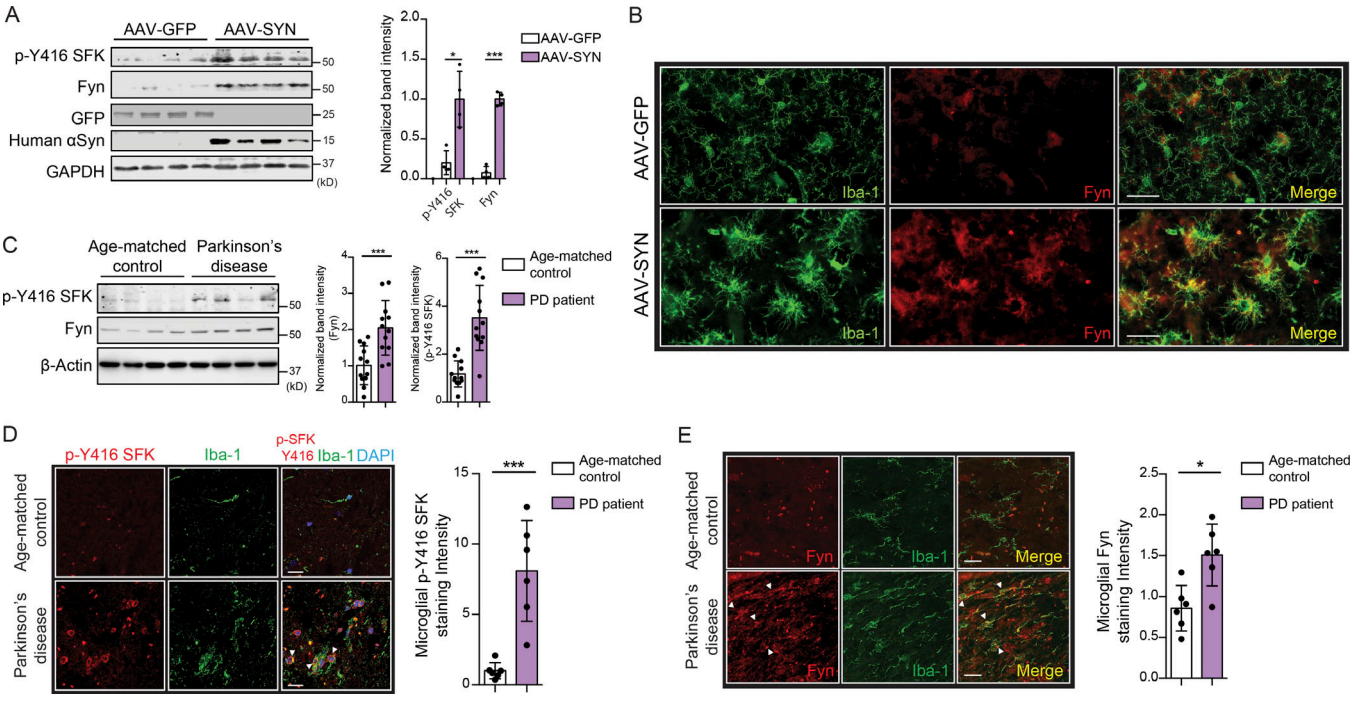

Figure 2. **Microglial Fyn activation in human PD brains. (A)** Significantly increased Fyn expression and activation were observed in AAV-SYN–injected nigral lysates, as assessed by immunoblots. Error bars represent mean ± SEM. Unpaired two-tailed t test (n = 4 mice per group). **(B)** IHC analysis revealed Fyn induction in Iba-1–positive microglia in AAV-SYN–injected nigral brain sections. Scale bars, 30 µm. **(C)** Significant increase in Fyn expression and activation in PD ventral midbrain lysates, when compared with age-matched control lysates. Representative immunoblot is shown. Error bars represent mean ± SEM. Unpaired two-tailed t test (n = 12). **(D)** IHC analysis of PD brain sections revealed strongly increased p-Y416 SFK expression within Iba-positive microglia when compared with age-matched non-PD brain sections. Error bars represent mean ± SEM. Unpaired two-tailed t test (n = 6). Scale bars, 15 µm. **(E)** IHC shows increased microglial Fyn expression in PD ventral midbrain sections. Scale bars, 15 µm. Error bars represent mean ± SEM. Unpaired two-tailed t test (n = 6). Asterisks indicate the level of statistical significance: *, P ≤ 0.05; ***, P ≤ 0.001.

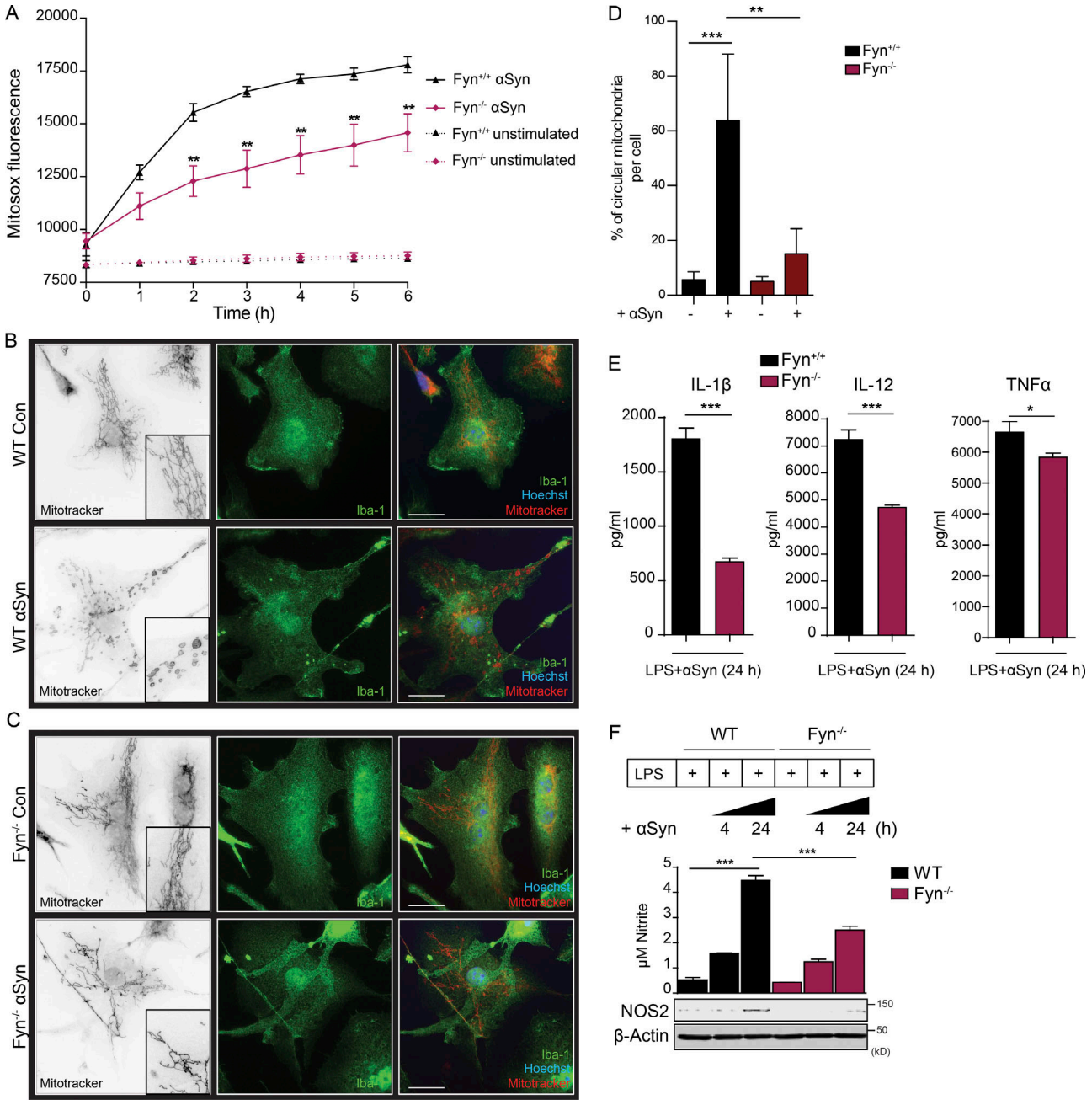

Figure 3. **Fyn-dependent αSyn uptake into microglial cells induces mitochondrial ROS generation. (A)** MitoSOX assay shows diminished mitoROS generation from αSyn-treated Fyn$^{-/-}$ microglia. Error bars represent mean ± SEM. One-way ANOVA followed by Tukey's post hoc test (n = 3). **(B and C)** ICC analysis reveals diminished mitochondrial morphology deficits observed in the aggregated αSyn-treated Fyn$^{-/-}$ microglia. Scale bars, 15 µm. Con, control. **(D)** Quantification of mitochondrial circularity. Error bars represent mean ± SEM. One-way ANOVA followed by Tukey's post hoc test (n = 3). **(E)** LPS-primed αSyn-treated WT microglia produced higher amounts of proinflammatory cytokines than Fyn-deficient microglia, as evidenced by Luminex supernatant analysis. Error bars represent mean ± SEM. Unpaired two-tailed t test (n = 4). **(F)** αSyn treatment induced the production of supernatant nitrite and NOS2, as evidenced by Griess assay and immunoblots, respectively, but did so to a significantly lesser extent in Fyn-deficient microglia. Error bars represent mean ± SEM. One-way ANOVA followed by Tukey's post hoc test (n = 3). Asterisks indicate the level of statistical significance: *, P ≤ 0.05; **, P ≤ 0.01; ***, P ≤ 0.001.

mitoROS to a significantly greater extent in WT microglia than in Fyn$^{-/-}$ microglia, presumably because of diminished αSyn uptake under Fyn$^{-/-}$ conditions (Fig. 3 A). Mitochondrial dysfunction in microglia alters mitochondrial morphology, resulting in increased circularity (Sarkar et al., 2017). αSyn-treated WT, but not Fyn$^{-/-}$, microglia exhibited a change in mitochondrial morphology, indicating fragmented mitochondria (Fig. 3, B–D). NLRP3 inflammasome priming occurs after NF-κB pathway activation (Hayden and Ghosh, 2004). The exact nature of the NLRP3 inflammasome activating signal remains contested. Lysosomal dysfunction and potassium efflux are implicated as potential activating agents. However, excessive mitoROS generation has now been accepted as the most important contributor to the activation of the NLRP3 inflammasome in various

models (Tschopp and Schroder, 2010; Zhou et al., 2011). Complex-I inhibition in mitochondria is sufficient to activate the NLRP3 inflammasome in LPS-primed microglia (Sarkar et al., 2017). To that end, we first checked whether αSyn could act as a danger signal to activate the LPS-primed NLRP3 inflammasome. Primary murine microglia primed with 100 ng/ml LPS for 3 h were treated with 500 nM aggregated αSyn for 24 h, with or without pretreatment with the pan-caspase inhibitor Z-VAD-FMK or the Casp-1–specific inhibitor Z-YVAD-FMK. αSyn induced IL-1β secretion in LPS-primed microglia, which was significantly reduced in the groups pretreated with caspase inhibitors (Fig. S2 A, left panel). In contrast, TNFα secretion in αSyn-treated LPS-primed cells did not significantly change and was only marginally reduced by Casp-1 and pan-caspase inhibition (Fig. S2 A, right panel). Next, we treated LPS-primed BMDMs from WT, NLRP3$^{-/-}$, ASC$^{-/-}$, Casp-1$^{-/-}$, and Casp-11$^{-/-}$ mice with 500 nM aggregated αSyn for 24 h (Fig. S2 B). αSyn-stimulated IL-1β secretion from NLRP3-, ASC-, and Casp-1–deficient BMDMs was dramatically reduced but only modestly attenuated in Casp-11–deficient BMDMs (Casp-11$^{-/-}$ BMDMs served as a control, since the Casp-1$^{-/-}$ mouse line inherently lacks Casp-11; Fig. S2 B, left panel). Supernatant levels of TNFα did not change significantly in any of the genotypes (Fig. S2 B, right panel). Immunoblotting revealed that a deficiency of NLRP3, ASC, Casp-1, or Casp-11 did not affect the levels of pro–IL-1β induced upon LPS treatment (Fig. S2 C). Inflammasome activation in vitro and in vivo is characterized by the formation of ASC specks (Stutz et al., 2013; Kuri et al., 2017; Venegas et al., 2017). LPS priming alone did not elicit ASC speck formation in primary microglia, but the number of LPS-primed cells displaying ASC puncta significantly increased after adding αSyn (Fig. S2, D and E). αSyn treatment of LPS-primed microglia also significantly induced the secretion of IL-1β, TNFα, and IL-12 as well as nitrite and NOS2 induction much more in WT than in Fyn$^{-/-}$ microglia (Fig. 3, E and F).

Aggregated αSyn primes and activates the NLRP3 inflammasome, resulting in IL-1β processing and secretion

Next, we tested whether aggregated αSyn could activate the NLRP3 inflammasome independent of an LPS priming step. Unprimed WT microglia were treated with αSyn alone or in combination with the NLRP3 inflammasome inhibitor MCC 950, the Casp-1 inhibitor Z-YVAD-FMK, and the Fyn kinase inhibitor saracatinib. αSyn induced robust IL-1β secretion, which was inhibited in a dose-dependent manner by all three pretreatments (Fig. 4 A, left panel). The secretion of TNFα was also reduced following saracatinib pretreatment, suggesting that Fyn might serve a broader role in mediating proinflammatory pathways (Fig. 4 A, right panel). We also treated unprimed, immortalized WT and Casp-1$^{-/-}$ microglial cells with aggregated αSyn for 4 and 6 h. As assessed via immunoblot, αSyn induced pro–IL-1β and NLRP3 expression equivalently in both cell types (Fig. 4 B). It also brought about the secretion of IL-1β in WT, but to a strikingly lower extent in Casp-1–deficient microglial cells (Fig. 4 C, left panel). TNFα secretion was unchanged (Fig. 4 C, right panel). αSyn treatment of WT, NLRP3$^{-/-}$, ASC$^{-/-}$, Casp-1$^{-/-}$, and Casp-11$^{-/-}$ BMDMs revealed no genotypic difference in their ability to induce pro–IL-1β and import αSyn (Fig. 4 D). However, the αSyn-mediated cleavage of Casp-1 was abrogated in ASC$^{-/-}$, NLRP3$^{-/-}$, and Casp-1$^{-/-}$ BMDMs. This was further evidenced using a Casp-1 immunoblot from 24-h αSyn-treated WT, NLRP3$^{-/-}$, ASC$^{-/-}$, and Casp-1$^{-/-}$ cell supernatants (Fig. 4 E). Furthermore, supernatant analysis of BMDMs treated with aggregated αSyn for 24 h showed that αSyn elicited robust IL-1β production from WT, but not NLRP3$^{-/-}$, ASC$^{-/-}$, and Casp-1$^{-/-}$ BMDMs, and was largely restored in the Casp-11$^{-/-}$ BMDMs (Fig. 4 F, left panel). αSyn-mediated TNFα production was not statistically different in any of the cell types (Fig. 4 F, right panel). To confirm that our findings held significance when applied to microglia, we confirmed that Casp-1– and NLRP3-deficient primary microglia did not secrete detectable levels of IL-1β in the supernatant when stimulated with αSyn (Fig. 4 G). To ensure that the inflammasome activation seen in our systems was independent of endotoxin contamination from our αSyn preps, we used endotoxin-free mouse αSyn to prime and activate WT microglia, with or without MCC 950 pretreatment for 24 h. Supernatant lysates were probed for Casp-1 via immunoblot and IL-1β secretion assayed via ELISA. αSyn was able to elicit a robust inflammasome response, which was strongly blocked with MCC 950 pretreatment (Fig. 4, H and I). αSyn treatment elicited the formation of large, single specks in the ASC-CFP reporter cell line, which overexpresses ASC tagged with CFP (Fig. 4 J). Heneka et al. (2013) conclusively demonstrated NLRP3 inflammasome activation in the APP/PS-1 AD model, as well as in postmortem AD brains, as indicated by increased levels of cleaved Casp-1. Accordingly, we detected significantly increased cleaved Casp-1 levels in the ventral midbrain lysates of 4-mo-old A53T mice compared with their littermate controls, indicating that αSyn aggregation/overexpression can elicit inflammasome activation in vivo (Fig. 4 K). Ventral midbrain lysates of AAV-SYN–injected mice also showed significantly increased Casp-1 p20 levels when compared with AAV-GFP lysates (Fig. 4 L). Lastly, both Casp-1 p20 and IL-1β levels were significantly increased in human PD ventral midbrain lysates when compared with those of control patients (Fig. 4 M). These data strongly suggest that αSyn itself can prime and activate the NLRP3 inflammasome in vitro and in vivo.

Fyn contributes to αSyn-induced NLRP3 inflammasome priming via PKCδ-mediated NF-κB activation

Previously, we described how Fyn kinase tyrosine phosphorylates PKCδ, feeding into the NF-κB pathway activation in microglia (Panicker et al., 2015). To determine whether Fyn plays a role in inflammasome priming, we treated WT and Fyn$^{-/-}$ primary microglia with various doses of LPS and TNFα for 3 h and blotted the lysates for pro–IL-1β and NLRP3, which were induced to discernably lower levels in Fyn$^{-/-}$ microglia (Fig. S3 A). We next treated Fyn$^{+/+}$ and Fyn$^{-/-}$ mice with 5 mg/kg LPS for 24 h and determined that LPS-mediated serum IL-1β production in Fyn$^{-/-}$ mice was strongly attenuated (Fig. S3 B).

Activation of the NF-κB pathway is characterized by nuclear translocation of its p65 subunit. To assess the role of Fyn in αSyn-mediated priming of the NLRP3 inflammasome, we

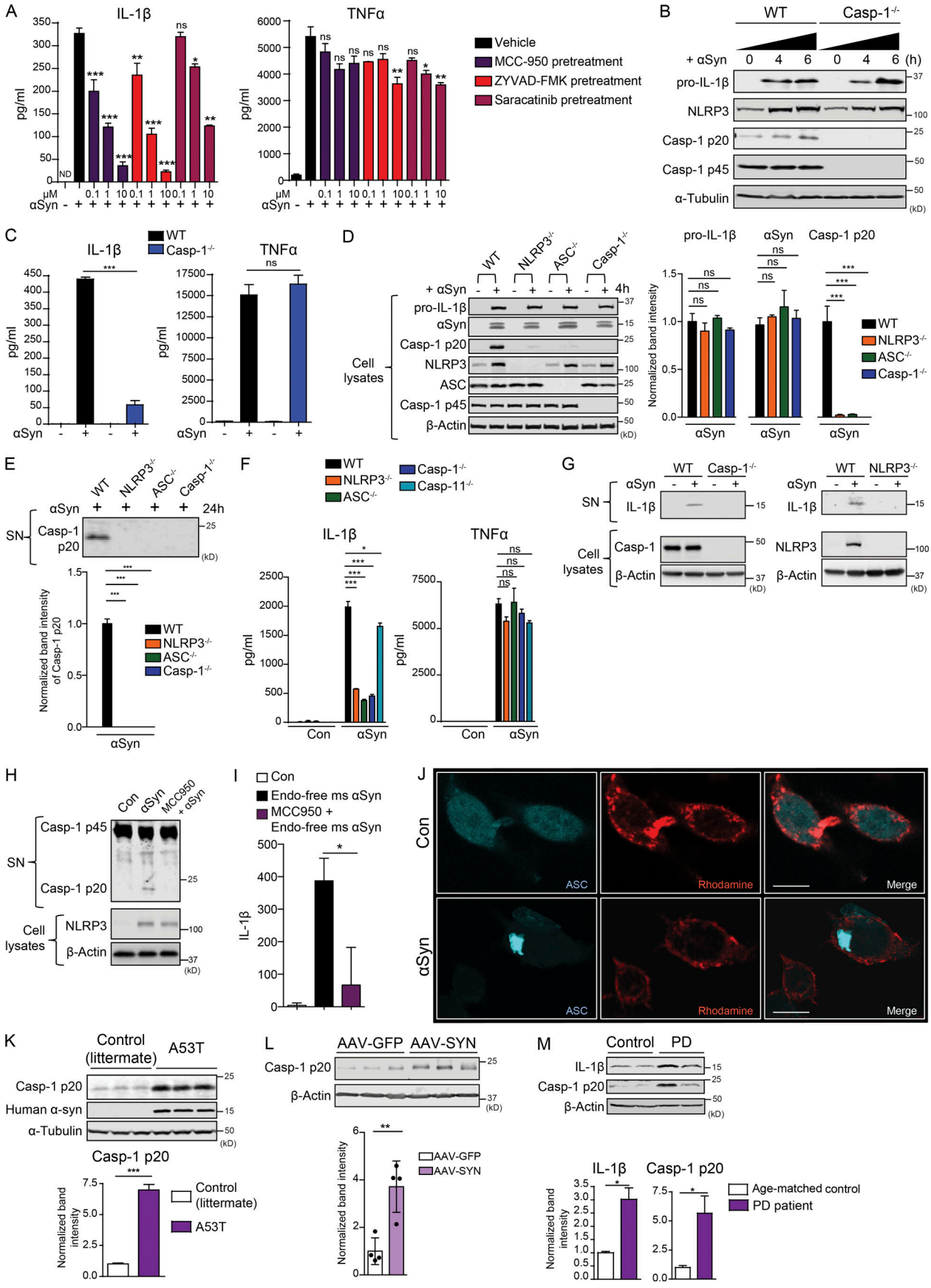

Figure 4. **αSyn can prime and activate the NLRP3 inflammasome to mediate IL-1β production. (A)** Luminex analysis shows that αSyn treatment elicited IL-1β production from unprimed microglial cells, which could be inhibited in a dose-dependent manner by inhibitors of the NLRP3 inflammasome, Casp-1 and Fyn. Fyn inhibition also inhibited αSyn-mediated TNFα production. Error bars represent mean ± SEM. One-way ANOVA followed by Tukey's post hoc test (n = 5). **(B)** αSyn induced Casp-1–independent induction of pro–IL-1β and NLRP3 levels, as evidenced by immunoblot analysis from αSyn-treated WT and Casp-1$^{-/-}$ microglial cell lysates. **(C)** Luminex analysis shows αSyn treatment induced Casp-1–dependent production of IL-1β, but not TNFα, from microglial cells. Error bars represent mean ± SEM. One-way ANOVA followed by Tukey's post hoc test (n = 3). **(D)** NLRP3$^{-/-}$, ASC$^{-/-}$, and Casp-1$^{-/-}$ BMDMs exhibited similar αSyn-induced production of pro–IL-1β and uptake of αSyn but almost completely attenuated Casp-1 cleavage, as shown by immunoblots. Error bars represent mean ± SEM. One-way ANOVA followed by Tukey's post hoc test (n = 3). **(E)** αSyn induced Casp-1 p20 secretion in WT, but not NLRP3$^{-/-}$, ASC$^{-/-}$, and Casp-1$^{-/-}$ BMDM supernatants, as shown by supernatant (SN) immunoblot. Error bars represent mean ± SEM. One-way ANOVA followed by Tukey's post hoc test (n = 3). **(F)** αSyn-mediated production of IL-1β, but not TNFα, was strongly attenuated in NLRP3$^{-/-}$, ASC$^{-/-}$, and Casp-1$^{-/-}$ but minimally affected in Casp-11$^{-/-}$ BMDM supernatants, indicating that αSyn both primes and activates the NLRP3 inflammasome primarily through its canonical activation, as shown by Luminex analysis. Error bars represent mean ± SEM. One-way ANOVA followed by Tukey's post hoc test (n = 5). Con, control. **(G)** Supernatant immunoblot analysis shows that WT, but not Casp1$^{-/-}$ and NLRP3$^{-/-}$ primary microglia, secrete IL-1β upon αSyn treatment. **(H)** Endotoxin-free aggregated mouse αSyn was able to elicit Casp-1 cleavage and secretion in WT microglia, and this was blocked with MCC 950 pretreatment. MCC 950 had no effect on NLRP3 induction in whole-cell lysates, as shown via immunoblots. **(I)** Endotoxin-free aggregated mouse αSyn was able to elicit IL-1β secretion from WT microglia, and this was substantially blocked upon MCC 950 pretreatment, as assessed via ELISA for IL-1β. Error bars represent mean ± SEM. One-way ANOVA followed by Tukey's post hoc test (n = 3). **(J)** ICC shows aggregated αSyn treatment induced ASC speck formation in the ASC-CFP reporter cell line. Scale bars, 15 µm. **(K)** Immunoblot analysis of 4-mo-old A53T nigral lysates revealed a significant increase in the levels of cleaved Casp-1 levels when compared with littermate controls. Bars represent mean ± SEM. Unpaired two-tailed t test (n = 4 mice per group). **(L)** Immunoblot analysis shows increased cleaved Casp-1 levels in AAV-SYN nigral lysates. Error bars represent mean ± SEM. Unpaired two-tailed t test (n = 4 mice per group). **(M)** Immunoblot analysis of PD nigral tissue lysates revealed significantly increased IL-1β and Casp-1 p20 levels when compared with age-matched control nigral lysates. Error bars represent mean ± SEM. Unpaired two-tailed t test (n = 3). Asterisks indicate the level of statistical significance: ns, not significant; *, P ≤ 0.05; **, P ≤ 0.01; ***, P ≤ 0.001.

treated WT and Fyn$^{-/-}$ primary microglia with aggregated αSyn for 15, 30, and 45 min and probed the lysates for p-Y311 PKCδ. αSyn treatment rapidly induced PKCδ activation in WT, but not in Fyn$^{-/-}$, microglia (Fig. 5 A). To examine whether Fyn and PKCδ contribute to αSyn-mediated NF-κB pathway activation, we prepared nuclear extracts from αSyn-treated WT, Fyn$^{-/-}$, and PKCδ$^{-/-}$ microglia. Immunoblot analysis revealed reduced p65 nuclear translocation in Fyn$^{-/-}$ and PKCδ$^{-/-}$ microglial nuclear lysates (Fig. 5, B and I). The αSyn-mediated induction of pro–IL-1β and NLRP3 mRNAs was reduced in Fyn$^{-/-}$ microglia (Fig. 5 C). Notably, αSyn treatment did not induce NLRC4 and AIM2 inflammasome levels, demonstrating that the NLRP3 inflammasome was preferentially activated. Immunoblot analysis revealed that pro–IL-1β, mature IL-1β, NLRP3, and cleaved Casp-1 levels were significantly diminished in αSyn-treated Fyn$^{-/-}$ microglia (Fig. 5 D). The αSyn-mediated induction of Casp-1 activity was induced in WT, but not Fyn-deficient, microglia, as verified by the FLICA Casp-1 activity assay (Fig. 5 E). We also knocked down Fyn using Fyn-specific siRNA and observed diminished induction of pro–IL-1β in αSyn-treated primary WT microglia (Fig. 5 F). Immunoblot and Luminex analyses of αSyn-treated microglial supernatants revealed diminished secretion of mature IL-1β and IL-12 from Fyn$^{-/-}$ cells (Fig. 5, G and H). As expected, the αSyn-mediated up-regulation of pro–IL-1β mRNA was also significantly attenuated in the PKCδ-deficient microglia (Fig. 5 J), as was the synthesis of pro–IL-1β (Fig. 5 K) and the production of supernatant IL-1β (Fig. 5 L). We also tested the role of PKCδ in αSyn import by using whole-cell lysates from WT and PKCδ$^{-/-}$ microglia treated with aggregated αSyn for 30 and 45 min. We saw no change between either genotype with respect to αSyn import (Fig. 5 M). These results suggest a bifurcation of the Fyn-dependent signaling pathway, showing that Fyn activation feeds into the PKCδ-dependent NF-κB pathway activation and priming of the NLRP3 inflammasome and the CD36-dependent but PKCδ-independent import of αSyn. CD36-deficient BMDMs also showed attenuated αSyn-induced p-Y311 PKCδ phosphorylation, pro–IL-1β induction, and IL-1β secretion when compared with WT BMDMs, showing that the αSyn-mediated priming and activation of the NLRP3 inflammasome occurred downstream of CD36 (Fig. S4).

Fyn kinase contributes to microgliosis and microglial inflammasome activation in the AAV-αSyn mouse model of PD

To verify Fyn's role in inflammasome activation in vivo, we used the AAV-SYN model at 45 d after injection (Fig. 6 A). Successive coronal brain sections were stained for tyrosine hydroxylase (TH) and GFP or human αSyn to verify that virus injections were correctly targeted to the SNpc as evidenced by a colocalization of the TH-positive dopaminergic neurons and the GFP or human αSyn (Fig. 6 B). As evidenced by the colocalization IHC analysis, neurons in the SNpc were targeted with accuracy, whereas dopaminergic neurons of the ventral tegmental area were relatively untargeted. This was intentional, since it is the degeneration of SNpc neurons that best characterizes PD neurodegeneration. Interestingly, a modest loss of TH-positive cells was evident within the SNpc of WT AAV-SYN–injected mice. In ventral midbrain sections stained for TH and Iba-1, massive nigral microgliosis was observed in WT, but not Fyn$^{-/-}$, AAV-SYN–injected mice (Fig. 6 C). To better visualize the degree of microgliosis, we used Imaris software to generate three-dimensional (3D) reconstructions of the Z-stack images (Fig. 6 D). AAV-SYN injection in WT mice elicited Iba-1–positive microglia accumulation in the SNpc as well as microgliosis, as quantified by an increase in Iba-1 staining intensity in WT, but not Fyn$^{-/-}$, mice (Fig. 6, E and F). A feature that validates activation of the inflammasome in vivo is the formation of ASC specks in the microglia, as has been demonstrated in the APP/PS1 mouse AD model (Heneka et al., 2013). Accordingly, we stained sections with antibodies to ASC and Iba-1 and quantified the number of microglial cells per field showing ASC specks. AAV-SYN–injected WT, but not Fyn$^{-/-}$, mice demonstrated a significant increase in the number of ASC speck–positive

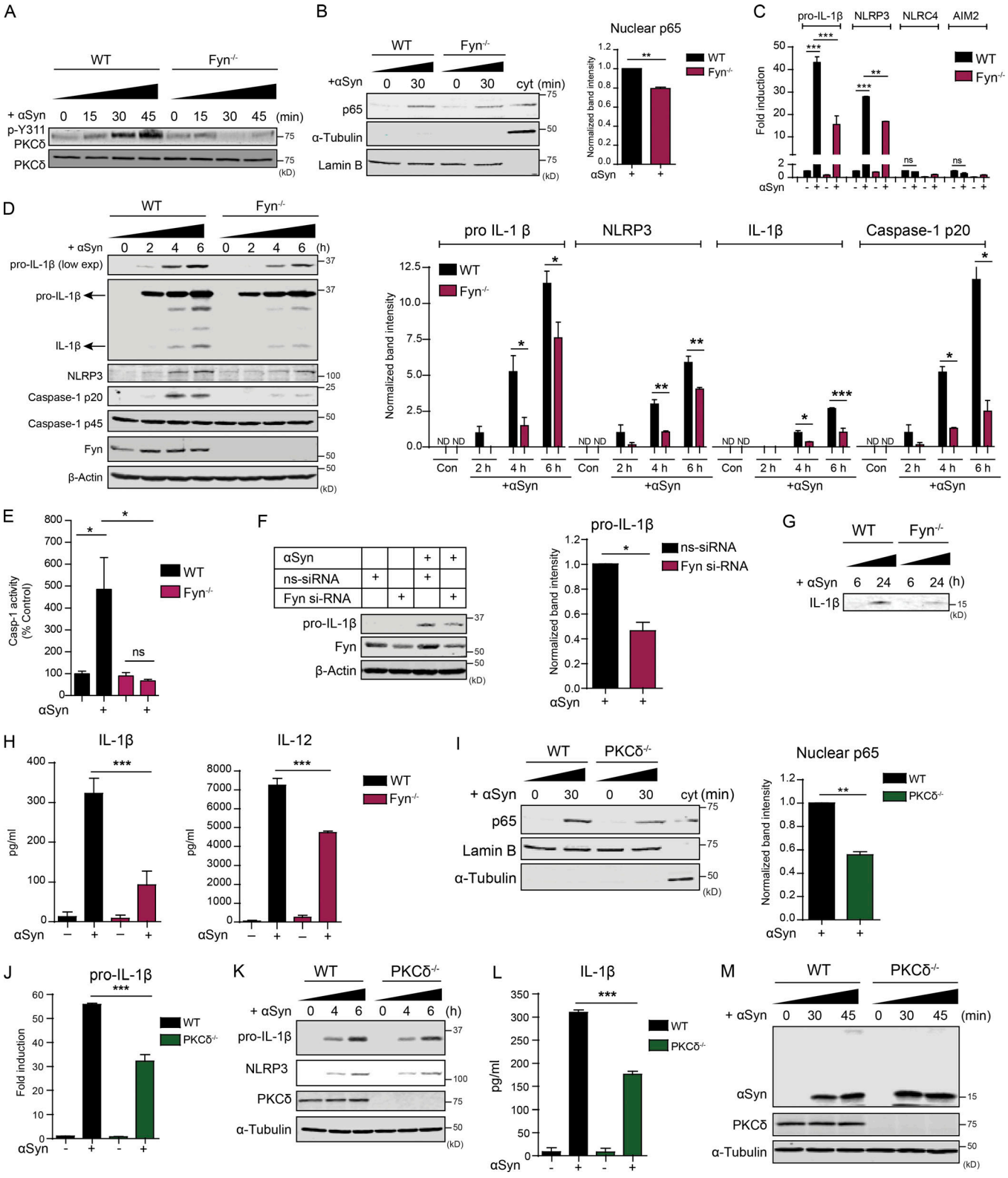

Figure 5. **Fyn contributes to αSyn-mediated priming of the NLRP3 inflammasome, resulting in diminished production of IL-1β and other pro-inflammatory cytokines. (A)** Immunoblot analysis of aggregated αSyn-treated WT and Fyn$^{-/-}$ microglial lysates reveals a rapid induction of pY311-PKCδ levels in WT, but not Fyn$^{-/-}$, microglia. **(B)** Diminished αSyn-induced nuclear translocation of NF-κB-p65 in Fyn$^{-/-}$ microglial cells, as shown by immunoblot analysis of nuclear fractions. Error bars represent mean ± SEM. Unpaired two-tailed *t* test (n = 3). **(C)** Diminished induction of pro–IL-1β and NLRP3 mRNA levels in Fyn-deficient microglia upon αSyn treatment, as shown by qRT-PCR. Error bars represent mean ± SEM. One-way ANOVA followed by Tukey's post hoc test (n = 3). **(D)** Reduced induction of pro–IL-1β and NLRP3 protein levels, as well as Casp-1 and IL-1β cleavage, in Fyn$^{-/-}$ microglia, as demonstrated by immunoblot analysis. Error bars represent mean ± SEM. One-way ANOVA followed by Tukey's post hoc test (n = 4). Con, control. **(E)** FLICA assay revealed

strongly increased Casp-1 activation in αSyn-treated WT, but not Fyn$^{-/-}$, microglia. Error bars represent mean ± SEM. One-way ANOVA followed by Tukey's post hoc test (n = 3). **(F)** Knocking down Fyn using siRNA reduces αSyn-mediated induction of pro–IL-1β in primary WT microglia, as shown by immunoblot. Error bars represent mean ± SEM. Unpaired two-tailed t test (n = 3). **(G and H)** Supernatant immunoblot and Luminex show reduced supernatant levels of IL-1β and other proinflammatory cytokines from αSyn-treated Fyn$^{-/-}$ microglia. Error bars represent mean ± SEM. One-way ANOVA followed by Tukey's post hoc test (n = 3). **(I)** Reduced aggregated αSyn-mediated p65 nuclear translocation seen in PKCδ$^{-/-}$ microglia, as shown by immunoblot analysis of nuclear fractions. Error bars represent mean ± SEM. Unpaired two-tailed t test (n = 3). **(J)** qRT-PCR shows attenuated αSyn-induced pro–IL-1β mRNA induction in PKCδ-deficient microglia. Error bars represent mean ± SEM. One-way ANOVA followed by Tukey's post hoc test (n = 3). **(K and L)** Reduced induction of pro–IL-1β and NLRP3 proteins (verified by immunoblot; K) and secretion of IL-1β (checked via Luminex; L) from PKCδ$^{-/-}$ microglia. Error bars represent mean ± SEM. One-way ANOVA followed by Tukey's post hoc test (n = 3). **(M)** No change in the import of aggregated αSyn observed between PKCδ$^{+/+}$ and PKCδ$^{-/-}$ microglia, as shown by immunoblot analysis. Asterisks indicate the level of statistical significance: ns, not significant; *, P ≤ 0.05; **, P ≤ 0.01; ***, P ≤ 0.001.

microglia (Fig. 7, A and B). Double staining of AAV-SYN–injected WT and Fyn$^{-/-}$ mouse ventral midbrain sections for NLRP3 and Iba-1 revealed diminished induction of microglial NLRP3 in the Fyn$^{-/-}$ mice (Fig. S5). To visualize the formation of ASC specks in the AAV-SYN model, confocal microscopy Z-stacks of ASC/Iba-1–stained sections were visualized in Imaris, where 3D reconstruction of the ASC staining pattern clearly demonstrated the presence of ASC specks within Iba-1–positive microglia in AAV-SYN–injected WT mice. Microglial ASC in AAV-SYN–injected Fyn$^{-/-}$ mice showed cytosolic localization with no speck formation (Fig. 7 C). The αSyn-mediated NLRP3 inflammasome activation pathway is summarized in Fig. 8.

Discussion

Increased neuroinflammation, mediated primarily by resident brain microglia is a well-acknowledged hallmark of PD. αSyn can induce microglial activation (Zhang et al., 2005), but the underlying signaling pathways that lead to microgliosis and specifically to microglial NLRP3 inflammasome activation in PD are poorly characterized. We first demonstrate rapid αSyn-mediated microglial Fyn activation in cell culture, as well as in the AAV-SYN model (Fig. 1, A–C).

Various receptors have been indirectly implicated in binding to and mediating αSyn signaling. Kim et al. (2013) considered TLR2 essential for αSyn-induced proinflammatory signaling and αSyn import into microglia. TLR4-, CD36-, and FcγR-deficient microglia have exhibited attenuated neuroinflammatory responses to αSyn treatment (Su et al., 2008; Cao et al., 2012; Fellner et al., 2013). Misfolded αSyn also interacts with microglial TLR1/2 and mediates Myd-88–dependent proinflammatory signaling (Daniele et al., 2015). Fyn activation can occur downstream of the class B scavenger receptor CD36 (Moore et al., 2002; Chen et al., 2008) as well as TLR2 (Finberg et al., 2012) in other cell types. We show that αSyn can interact with the microglial receptors TLR2 and CD36 in microglia (Fig. 1, D and E). Immunoprecipitation analysis revealed a transient interaction between CD36 and αSyn, one that may allow αSyn entry into microglia (Fig. 1 E). Since immunoprecipitation-based interactions of αSyn with its potential microglial receptors, including TLR2, have proven difficult to accomplish in the past (Kim et al., 2013), we posit that the transient nature of its interaction with receptors (CD36 and αSyn interaction was only observed at 15 and 30 min after treatment, not after) may preclude identification of its binding partners. Concordant with this hypothesis, the uptake of αSyn was significantly attenuated in CD36-deficient BMDMs, as well as Fyn-deficient microglia (Fig. 1, F–K). Recent GWASs indicate an association of the FYN locus with risk of PD (Nalls et al., 2018 *Preprint*). We observed induction and activation of Fyn within Iba-1–positive microglia using the AAV-αSyn mouse model, as well as in the PD brain (Fig. 2). This is the first paper that demonstrates an induction of Fyn in PD mouse models and, especially in light of its association with human PD, might prove to have pathological and/or therapeutic significance.

αSyn elicits mitochondrial deficits in neurons. Defective mitochondria produce excessive mitoROS as a result of ineffective mitochondrial respiration. MitoROS generation has now been accepted as a key contributor to the activation of the NLRP3 inflammasome (Tschopp and Schroder, 2010; Zhou et al., 2011). αSyn treatment elicited mitoROS generation and concomitant mitochondrial circularization in WT, but not Fyn$^{-/-}$, microglia (Fig. 3, A–C).

Misfolded proteins have been shown to activate LPS-primed NLRP3 inflammasome in microglia (Halle et al., 2008; Hafner-Bratkovič et al., 2012). We demonstrate that αSyn can elicit IL-1β production in LPS-primed microglia by activating the NLRP3 inflammasome, as evidenced by the Casp-1–, NLRP3-, and ASC-dependent production of IL-1β (Fig. S2, A and B). A major finding of this paper is that αSyn can serve as both a priming and activating agent to assemble the NLRP3 inflammasome in microglia. Thus far, in most major NLRP3 inflammasome studies, the fulfillment of these two steps has been accomplished by two disparate agents, with LPS usually used for priming. This has limited significance in human disease, because progressive protein aggregation diseases like AD and PD do not entail the presence of LPS. Since αSyn can serve both steps to elicit NLRP3 inflammasome assembly and activation, we believe that this portends its significance as a pathology-inducing entity.

αSyn treatment of unprimed microglia resulted in robust IL-1β production, which was inhibited in a dose-dependent manner by inhibitors of the NLRP3 inflammasome (MCC-950), Casp-1 (Z-YVAD-FMK), and Fyn (saracatinib; Fig. 4 A). IL-1β secretion was also strongly attenuated in immortalized Casp-1$^{-/-}$ microglia when compared with WT microglial cells (Fig. 4, B and C). MCC-950 pretreatment reduced IL-1β secretion in microglia by ∼85% but did not abolish it entirely. MCC-950 prevents the activation of the canonical NLRP3 inflammasome, but not NLRC4, NLRP1, and noncanonical inflammasomes. Hence, our results suggest that while canonical activation of the NLRP3 inflammasome accounts for the bulk (80–85%) of the αSyn-mediated IL-1β secretion in microglia, activation of an alternate inflammasome

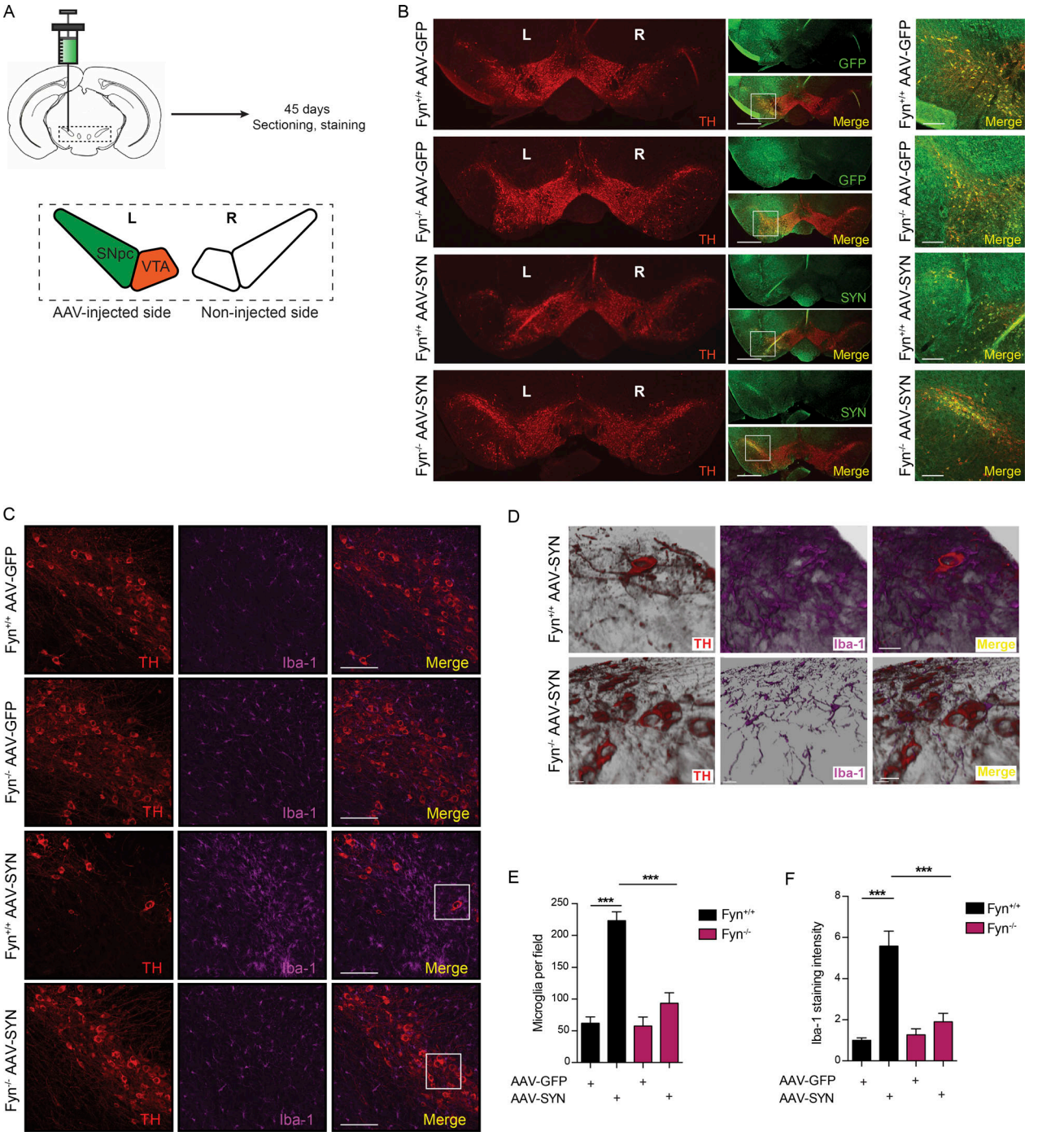

Figure 6. **Diminished microgliosis activation in Fyn-deficient mice using the AAV-SYN PD model**. **(A)** Representational diagram of AAV injection site in mice (left [L] and right [R]). VTA, ventral tegmental area. **(B)** Stereotaxic injection of AAV-GFP– and AAV-SYN–overexpressing particles into the SNpc resulted in specific targeting of SNpc dopaminergic neurons, as indicated by a colocalization of TH and GFP/human αSyn expression. Scale bars, 500 µm (left panel) and 100 µm (right panel). **(C)** IHC analysis shows massive microgliosis within the SNpc of $Fyn^{+/+}$ mice injected with the AAV-SYN particles, but not in $Fyn^{-/-}$ mice. Scale bars, 100 µm. **(D)** 3D reconstruction of the Z-stack images in the ventral midbrain of AAV-SYN–injected WT and $Fyn^{-/-}$ reveals contrasting microglial response between the genotypes. Scale bars, 20 µm. **(E)** Quantification of the number of microglia per field in the SNpc in AAV-GFP– or AAV-SYN–injected $Fyn^{+/+}$ and $Fyn^{-/-}$ ventral midbrain sections. Error bars represent mean ± SEM. One-way ANOVA followed by Tukey's post hoc test (n = 5 mice per group). **(F)** Quantification of the number of microglia Iba-1 staining intensity in the SNpc in AAV-GFP– or AAV-SYN–injected $Fyn^{+/+}$ and $Fyn^{-/-}$ ventral midbrain sections. Error bars represent mean ± SEM. One-way ANOVA followed by Tukey's post hoc test (n = 5 mice per group). Asterisks indicate the level of statistical significance: ***, $P \leq 0.001$.

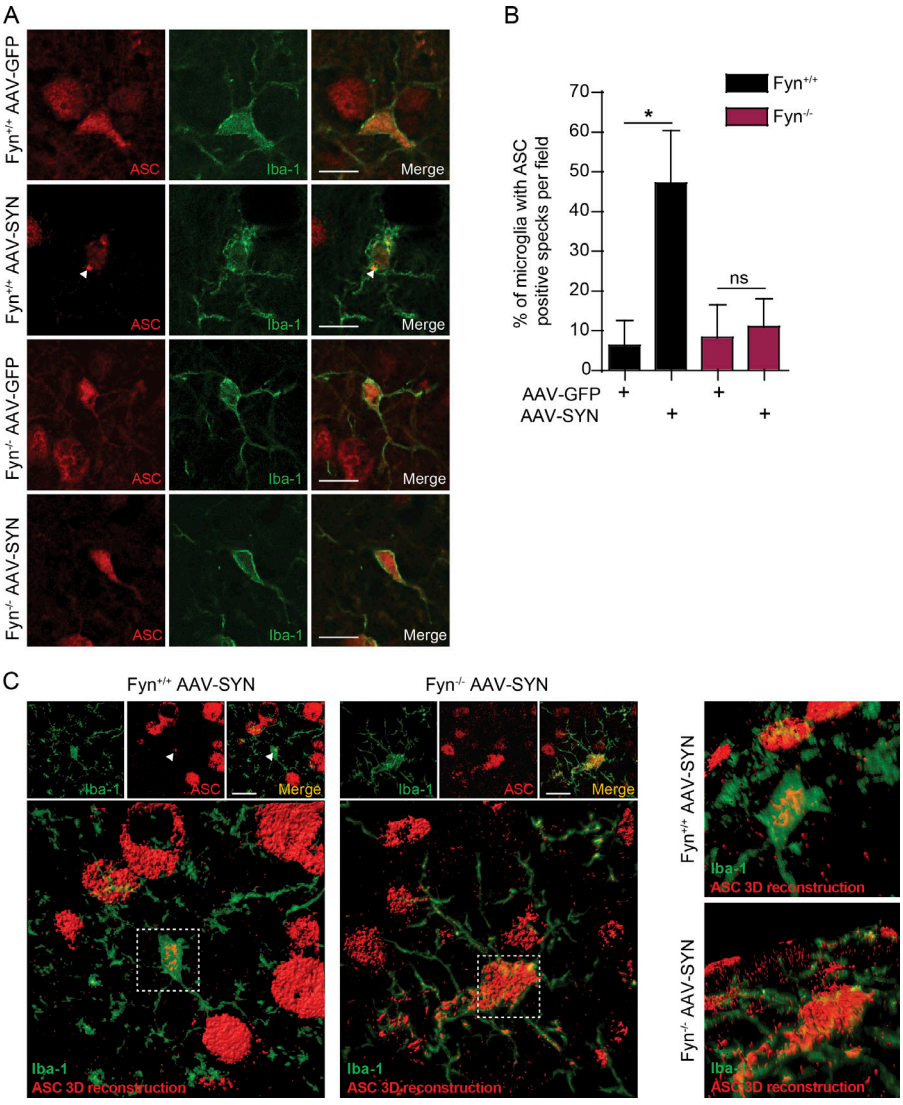

Figure 7. **Reduced αSyn-induced NLRP3 inflammasome activation in Fyn-deficient mice.** **(A)** AAV-SYN injection in $Fyn^{+/+}$, but not $Fyn^{-/-}$, mice elicits microglial ASC speck formation in the ventral midbrain, as seen by double IHC for Iba-1 and ASC. Scale bars, 15 µm. **(B)** Quantification of the midbrain ASC specks upon AAV-GFP or AAV-SYN injection in $Fyn^{+/+}$ and $Fyn^{-/-}$ ventral midbrain sections. Error bars represent mean ± SEM. One-way ANOVA followed by Tukey's post hoc test (n = 5 mice per group). **(C)** 3D reconstruction of microglial ASC expression in AAV-SYN–injected $Fyn^{+/+}$ and $Fyn^{-/-}$ mouse ventral midbrain sections. Asterisks indicate the level of statistical significance: *, $P \le 0.05$; ns, not significant. Scale bars, 15 µm.

may account for the remainder. Recently, dual activation of the NLRP3 and NLRC4 inflammasomes was demonstrated in microglia and astrocytes in a lysophosphatidylcholine model of multiple sclerosis, wherein NLRP3- and ASC-deficient astrocytes display strongly reduced, but not completely abolished, production of IL-1β, strongly reminiscent of our results (Freeman et al., 2017). However, the secretion of residual IL-1β under Casp-1 inhibition/knockout conditions suggests that even though canonical NLRP3 inflammasome activation accounts for the majority of αSyn-induced IL-1β release, a small portion of it occurs via Casp-1–independent mechanisms. Inflammasome-independent production of IL-1β has been demonstrated in osteomyelitis model systems (Lukens et al., 2014) and in response to *Mycobacterium tuberculosis* (Mayer-Barber et al., 2010). However, since Casp-1–independent IL-1β only accounts for a small fraction of the total IL-1β produced in response to αSyn, further investigations into the mechanisms that mediate Casp-1–independent IL-1β secretion should be investigated in a future study.

Next, we showed that BMDMs from $NLRP3^{-/-}$, $ASC^{-/-}$, and $Casp\text{-}1^{-/-}$ mice had negligible αSyn-induced Casp-1 activation (Fig. 4, D and E). αSyn-mediated secretion of IL-1β, but not TNFα, was greatly diminished in cell supernatants obtained from these cells, but not from cells obtained from $Casp\text{-}11^{-/-}$ mice (Fig. 4 F). We used $Casp\text{-}11^{-/-}$ BMDMs in this study, since $Casp\text{-}1^{-/-}$ mice were developed using an S129 mouse background, and these mice inherently lack Casp-11 expression. Gustin et al. (2015) indicated that commercially obtained aggregated αSyn could not elicit IL-1β production, but their finding has been refuted by multiple studies using recombinant endotoxin-free αSyn to elicit microglial IL-1β production (Lee et al., 2010; Boza-Serrano et al., 2014; Daniele et al., 2015), although these studies did not prove direct involvement of the NLRP3 inflammasome. To confirm that endotoxin contamination of our αSyn preparations did not lead to NLRP3 inflammasome activation, we used endotoxin-free mouse αSyn and showed that it could prime and activate the NLRP3 inflammasome, leading to IL-1β secretion in an NLRP3 inflammasome–dependent manner (Fig. 4, H and I). Endotoxin removal did not affect αSyn-mediated IL-1β secretion from microglia (Fig. 4, A and I). Since we made some inferences from studies based on BMDMs, we confirmed that αSyn treatment of

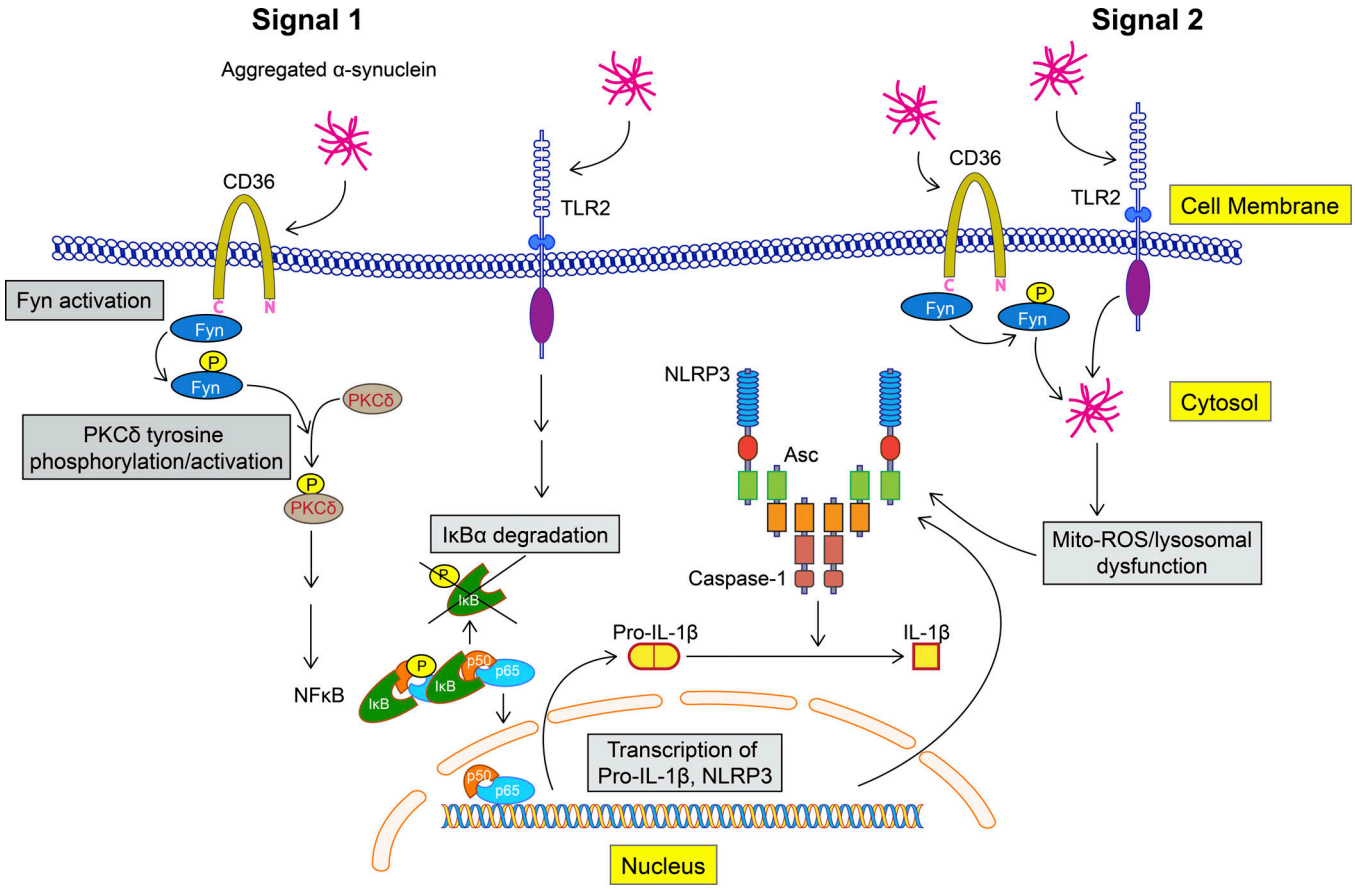

Figure 8. **Aggregated αSyn-mediated NLRP3 inflammasome activation pathway.** αSyn binds to the receptors TLR-2 and CD36 on microglial cells. CD36 recruits Fyn kinase, which is activated, and subsequently tyrosine phosphorylates PKCδ at Y311, leading to increased PKCδ-dependent activation of the NF-κB pathway. p65 translocates to the nucleus and brings about the induction of pro–IL-1β and NLRP3 mRNAs. Aggregated αSyn is taken up by the microglia, after which it brings about mitochondrial dysfunction–mediated activation of the NLRP3 inflammasome. Fyn, but not PKCδ, contributes to this process as well.

WT, but not Casp-1– and NLRP3-deficient, primary microglia elicited supernatant IL-1β secretion, as evidenced by immunoblot analysis (Fig. 4 G). A terminal readout of the NLRP3 inflammasome is the formation of ASC specks. We confirmed that αSyn treatment elicited ASC speck formation in the ASC-CFP macrophage cell line (Fig. 4 J).

Apart from microglia, αSyn also induces IL-1β production in monocytes (Codolo et al., 2013; Gustot et al., 2015). However, monocytes have constitutively activated Casp-1 (Netea et al., 2009). Because of this, pathways identified using these systems might not be relevant to resident microglial cells. We also demonstrate that NLRP3 inflammasome activation might have in vivo and clinical relevance. Cleaved Casp-1 levels increased markedly in nigral lysates of A53T and nigral lysates of AAV-SYN mice (Fig. 4, K and L), while levels of cleaved IL-1β and Casp-1 increased significantly in PD ventral midbrain lysates (Fig. 4 M). Although both these latter events were previously demonstrated in PD tissues (Mogi et al., 1996, 2000), these prior observations were made before the roles of these proteins were established within the context of inflammasome activation.

Since NLRP3 inflammasome priming involves induction of pro–IL-1β and NLRP3 following NF-κB activation, we reasoned that Fyn might contribute to this process as well, since we previously demonstrated its role in PKCδ-mediated NF-κB activation (Panicker et al., 2015). We show that the induction of NLRP3 and pro–IL-1β following LPS and TNFα treatment was significantly reduced in Fyn$^{-/-}$ microglia (Fig. S3 A). Fyn$^{-/-}$ mice also demonstrated diminished serum IL-1β response to intraperitoneal LPS administration (Fig. S3 B). αSyn treatment in microglia rapidly resulted in Fyn-dependent PKCδ Y311 phosphorylation in microglia (Fig. 5 A). The nuclear translocation of p65-NF-κB was reduced in both Fyn$^{-/-}$ and PKCδ$^{-/-}$ microglia (Fig. 5, B and I), as was the induction of pro–IL-1β mRNA (Fig. 5, C, and J) and protein (Fig. 5, D and K) and the secretion of mature IL-1β (Fig. 5, G, H, and L). The reduction in IL-1β secretion was more evident in Fyn-deficient microglia, presumably because Fyn played a role in both inflammasome priming and activation, whereas PKCδ only contributed to inflammasome priming. Knockdown of Fyn expression via siRNA reduced αSyn-mediated induction of pro–IL-1β in WT microglia (Fig. 5 F). Expectedly, PKCδ$^{-/-}$ microglia showed no deficits in αSyn uptake (Fig. 5 M). The experiments involving Fyn- and PKC-deficient microglia were performed using separate WT mouse strains. This is because PKCδ$^{+/+}$ mice were originally developed on a C57BL/6 background, whereas Fyn$^{+/+}$ mice originated from an S129 background, which inherently lacks Casp-11 expression.

Casp-11 participates in the activation of a noncanonical inflammasome (Kayagaki et al., 2011). Hence, we thought it prudent to use separate WT microglia for each genotype. From our results, both WT strains have nearly identical IL-1β responses to αSyn. Since Fyn lies downstream of CD36 in our signaling mechanism, we confirmed that αSyn-mediated PKCδ activation, inflammasome priming, and IL-1β secretion were significantly dampened in CD36-deficient BMDMs (Fig. S4). Switching to the AAV-SYN model, we observed significant microgliosis and microglial ASC speck formation in the ventral midbrain of $Fyn^{+/+}$, but not $Fyn^{-/-}$, mice (Figs. 6 and 7). There was also less microglial NLRP3 induction in AAV-SYN–injected $Fyn^{-/-}$ mice when compared with $Fyn^{+/+}$ mice (Fig. S5). This provides in vivo support to our findings that Fyn contributes to microglial inflammatory signaling with relevance to PD (Fig. 8). AAV-GFP infection alone has been shown to induce mild neurotoxicity over time, with previous reports showing 15% neuron loss at 12 wk after injection (Gombash et al., 2013). Inhibition of the NLRP3 inflammasome was recently investigated as a potential strategy to limit pathology in neurodegenerative diseases. Identifying the signaling mechanisms through which this complex is assembled is, in our view, the next step in unraveling how its activation can be curtailed. To the best of our knowledge, this is the first study that maps a molecular pathway that demonstrates how αSyn mediates simultaneous inflammasome priming and activation in models of PD. The identification of Fyn as an active contributor to both these processes holds particular significance, especially with the revelation of the *FYN* gene as a novel PD-associated locus. Future studies will investigate the role that Fyn plays in nonmicroglial cells in contributing to disease progression in PD.

Inhibitors of the NLRP3 inflammasome and Fyn have been used with success to control the progress of experimental autoimmune encephalitis and AD, respectively (Coll et al., 2015; Kaufman et al., 2015). Hence, it is conceivable that similar inhibitors could be used to halt the progression of PD.

Materials and methods

Chemicals and reagents

DMEM/F-12, ascorbic acid, RPMI 1640 medium, FBS, L-glutamine, Hoechst nuclear stain, penicillin, streptomycin, and other cell culture reagents were purchased from Invitrogen. L929 conditioned medium was a kind gift from Douglas Jones at Iowa State University (Ames, IA). Recombinant TNFα was purchased from PeproTech, and LPS (*Escherichia coli* 0111:B4, endotoxin content 6.6000000 EU/mg) and 6-OHDA were purchased from Sigma-Aldrich. The rabbit antibody to human αSyn were obtained from EMD Millipore. The MitoTracker Red and MitoSOX dyes were obtained from Life Technologies. Goat IL-1β, rat NLRP3, goat CD36, and TLR2 antibodies were obtained from R&D Systems. Mouse NLRP3, mouse Casp-1, and rabbit ASC antibodies were obtained from Adipogen. The mouse Fyn and GAPDH antibodies, as well as the Rhodamine Phalloidin stain were purchased from Thermo Fisher Scientific. Antibodies for rabbit Fyn, PKCδ, p-Y311 PKCδ, IκBα, Lamin-B, NOS2 (iNOS), mouse tubulin, and human αSyn were purchased from Santa Cruz Biotechnology. Antibodies against the rabbit p-Y416 SFK and native p65 were purchased from Cell Signaling. The TH antibody was purchased from Chemicon. Mouse M2 FLAG and β-actin antibodies as well as the rabbit β-actin antibody were purchased from Sigma-Aldrich. Rabbit and goat Iba-1 antibodies were purchased from Wako Chemicals and Abcam, respectively. The rat Casp-11 antibody was purchased from Novus Biologicals. FLAG-tagged human CD36 expressing plasmid was obtained from Sino Biological. The Bradford protein assay kit was purchased from Bio-Rad Laboratories. FLAG-tagged human WT Fyn and Y417A mutant Fyn constructs were obtained as described previously (Kaspar and Jaiswal, 2011). GFP and human αSyn–overexpressing adeno-associated viruses (GFP-AAV and SYN-AAV, respectively) were obtained from the University of North Carolina Viral Vector Core. The titers were 0.95×10^{13} and 10^{13} viral particles per milliliter, respectively. Both viral vectors were of the AAV-5 serotype and coded for GFP and human αSyn, respectively, under a chicken β-actin promoter. The WT and $Casp\text{-}1^{-/-}$ microglial cell lines and the ASC-CFP cell line were a gift from Dr. Douglas Golenbock at the University of Massachusetts (Worcester, MA). Femurs from WT, $NLRP3^{-/-}$, $ASC^{-/-}$, $Casp\text{-}1^{-/-}$, and $Casp\text{-}11^{-/-}$ mice were obtained from Dr. Leslie Freeman and Dr. Jenny P.Y. Ting at the University of North Carolina (Chapel Hill, NC). Apart from the Department of Pathology at Johns Hopkins, PD and age-matched brain sections were obtained from the University of Miami Brain Endowment Bank. CD36-, NLRP3-, and Casp-1–deficient mice were procured from Jackson Laboratories. NLRP3- and Casp-1–deficient mice, developed on a C57BL/6 background, were crossed in-house to C57BL/6 WT mice to obtain respective heterozygous mice, and these were interbred to obtain NLRP3-WT, Casp1-WT, $NLRP3^{-/-}$, and $Casp1^{-/-}$ pups. For primary microglial experiments, littermate control mice were used as WT mice.

Human αSyn purification and aggregation

BL21 (DE3) cells transformed with a pT7-7 plasmid encoding WT human αSyn were freshly grown on an ampicillin agar plate. Then a single colony was transferred to 10 ml of Luria broth medium with 100 µg/ml ampicillin incubated overnight at 37°C with shaking (preculture). The next day, the preculture was used to inoculate 1 liter of Luria broth/ampicillin medium. When the OD_{600} of the cultures reached 0.5, protein expression was induced with 1 mM isopropyl β-D-1-thio-galactopyranoside (Invitrogen), and the cells were further incubated at 37°C for 8 h before harvesting by centrifugation. Lysis was performed on ice by resuspending the cell pellet in 10 mM Tris-HCl, pH 8.0, 1 mM EDTA, and 1 mM PMSF and ultrasonicated with 30-s pulses followed by a 30-s pause, for a total ultrasonication time of 2 min. Lysates were finally filtered through 0.22-µm membranes and loaded onto a Bio-Rad UNO Q6 ion exchange column on a Biological DuoFlow (Bio-Rad Laboratories) chromatography system. Fractions eluted with a salt gradient were assayed for the presence of αSyn protein by SDS-PAGE followed by Coomassie staining. Fractions containing αSyn were pooled, dialyzed against 10 mM Hepes, pH 7.4, and 50 mM NaCl for protein concentration determination by Bradford assay.

Endotoxin-free mouse αSyn purification and aggregation

Recombinant mouse αSyn proteins were purified as previously described (Mao et al., 2016). Bacterial endotoxin was removed using the ToxinEraser endotoxin removal kit (GenScript). Following the manufacturer's instructions, αSyn was prepared in PBS to 5 mg/ml by agitating at 1,000 rpm at 37°C. Aggregated αSyn was stored at −80°C until use. The endotoxin levels post ToxinEraser treatment were 0.08 EU/μg protein. All batches of αSyn were found to have endotoxin levels of <0.5 EU/μg protein.

Animal studies

The $Fyn^{+/+}$ and $Fyn^{-/-}$ mice used in these studies were bred in our animal facility. $Fyn^{-/-}$ mice were originally obtained from Dr. Dorit Ron's laboratory at the University of California, San Francisco, and are available from the Jackson Laboratory (stock number 002271). The $Fyn^{+/+}$ and $Fyn^{-/-}$ mice used for the AAV studies were littermates. Commercial C57BL/6 WT mice were not used for animal studies with $Fyn^{-/-}$ mice. $PKC\delta^{-/-}$ mice were obtained originally from Dr. Keiichi Nakayama's laboratory (Division of Cell Biology, Department of Molecular and Cellular Biology, Medical Institute of Bioregulation, Kyushu University, Fukuoka, Japan). The human αSyn–overexpressing A53T mice were obtained from the Jackson Laboratory (B6.Cg-Tg(Prnp-SNCA*A53T)23Mkle/J, stock number 006823). Mice were housed under standard conditions of constant temperature (22 ± 1°C), humidity (relative, 30%), and a 12-h light cycle with food and water provided ad libitum. 6–8-wk-old male mice were used for all studies. Stereotaxic injection of the GFP-AAV and SYN-AAV particles into the SNpc was performed using the Angle 2 stereotaxic apparatus (Leica Biosystems). The coordinates, relative to bregma, were anteroposterior −3.1 mm, mediolateral −1.2 mm, and dorsoventral 4.0 mm.

Primary microglial cultures and treatments

Primary microglial cultures were prepared from WT, $Fyn^{-/-}$, and $PKC\delta^{-/-}$ postnatal day 1 mouse pups as described previously with slight modifications (Gordon et al., 2011; Panicker et al., 2015). Briefly, harvested mouse brains had their meninges removed before being placed in DMEM/F12 supplemented with 10% heat-inactivated FBS, 50 U/ml penicillin, 50 μg/ml streptomycin, 2 mM L-glutamine, 100 μM nonessential amino acids, and 2 mM sodium pyruvate. Brain tissues were then gently agitated for 15 min in 0.25% trypsin-EDTA. The trypsin reaction was stopped by adding double the volume of DMEM/F12 complete medium and then washing brain tissues three times. Tissues were then triturated gently to prepare a single-cell suspension, which was then passed through a 70-μm nylon mesh cell strainer to remove tissue debris and aggregates. The cell suspension was then made up in DMEM/F12 complete medium and seeded into T-75 flasks, which were incubated in humidified 5% CO_2 at 37°C. The medium was changed after 5–6 d, and the mixed glial cells were grown to confluence. Microglial cells were separated from confluent mixed glial cultures by differential adherence and magnetic separation to >97% purity and then were allowed to recover for 48 h after plating. Primary microglia in DMEM/F12 complete medium containing 2% FBS were primed with 1 μg/ml LPS for 3 h, which is a dose and time point used in several published studies (Halle et al., 2008). For signaling experiments, we used the protocol of Stuart et al. (2007), with slight modification. For this, primary microglial cells were kept in 2% DMEM/F12 complete medium for 5 h at 37°C before treatment with 3.5–7 μg/ml aggregated αSyn, which is similar to doses used by several published articles (Kim et al., 2013; Boza-Serrano et al., 2014). For ICC, microglia were obtained by the shake-off method as previously described (Gordon et al., 2011).

HEK-293 cell culture and transfection

HEK-293T cells were cultured in DMEM (Gibco, Thermo Fisher Scientific) supplemented with 10% FBS (Gibco, Thermo Scientific), penicillin, and streptomycin. Cells were cultured at 37°C with 5% CO_2. Transfection was performed using PolyFect reagent (Qiagen) according to the manufacturers' instructions. Typically, 2×10^5 cells per well in 6-well dishes were transfected with appropriate plasmids.

Primary BMDM cultures

A sterile blade was used to remove femoral epiphyses to expose the marrow cavity. A 30-gauge, 1/2-inch needle attached to a 10-ml syringe filled with 10% FBS-containing DMEM was used to flush marrow from the bone into a sterile 14-ml Falcon tube. The marrow was centrifuged at 250 ×*g* for 15 min at 4°C. Pellets were resuspended in bone marrow macrophage medium (DMEM containing 20% FBS, 30% L929 cell conditioned medium, penicillin/streptomycin, and sodium pyruvate), and 15×10^6 cells were plated out in Petri dishes (15 mm × 150 mm). Cell cultures were kept at 37°C and 5% CO_2 and supplemented with additional bone marrow macrophage medium on day 3, and then adherent differentiated macrophages were trypsinized on day 6 for experiments.

Immunoblotting

Brain tissue and cell culture lysates were prepared using modified RIPA buffer and were normalized for equal amounts of protein using the Bradford protein assay kit. Equal amounts of protein (6–10 μg for nuclear lysates, 10–25 μg for cell lysates, and 30–40 μg for tissue lysates) were loaded for each sample and separated on either 12% or 15% SDS-PAGE gels depending on the molecular weight of the target protein. After separation, proteins were transferred to a nitrocellulose membrane, and the nonspecific binding sites were blocked for 1 h using a blocking buffer specifically formulated for fluorescent Western blotting (Rockland Immunochemicals). Membranes were then probed with the respective primary antibodies for 3 h at room temperature (RT) or overnight at 4°C. Incubated membranes were washed seven times with PBS containing 0.05% Tween-20, and then secondary IR-680–conjugated anti-mouse (1:10,000; Molecular Probes) and IR-800–conjugated anti-rabbit (1:10,000; Rockland Immunochemicals) antibodies were used for detection with the Odyssey IR imaging system (LI-COR). Antibodies for GAPDH, β-actin and tubulin were used as loading controls. Antibodies against Lamin B were used as the loading control for nuclear lysates. We added 400 μl methanol and 100 μl chloroform to 400 μl of cell supernatants obtained after treatment from microglial cells treated in 12-well plates. The samples were

vortexed vigorously for 30 s and then centrifuged at 13,000 ×*g* for 5 min. The aqueous phase was removed via vacuum. The pellets were dried for 5–10 min at 55°C and subsequently reconstituted in 32 µl of 1× SDS sample buffer and 8 µl β-mercaptoethanol. The samples were then vortexed, boiled for 5 min, and used for immunoblotting for IL-1β.

Quantitative RT-PCR (qRT-PCR)

The RNA extraction protocol was adapted and modified from a published protocol (Seo et al., 2014). After mixed glial separation, we plated 2.5 × 10^6 microglia per treatment group in a 6-well plate. RNA was extracted after treatment using the TRIzol chloroform extraction method. We converted 1 µg of RNA to cDNA using a High Capacity cDNA Reverse Transcription kit from Applied Biosystems (4368814) following the manufacturer's protocol. qRT-PCR was performed on the following genes using SYBR Green qPCR Mastermix from Qiagen (208056): NLRP3 forward, 5′-TGCTCTTCACTGCTATCAAGC CCT-3′; NLRP3 reverse, 5′-ACAAGCCTTTGCTCCAGACCCTAT-3′ (synthesized in Iowa State University's DNA facility) and IL-1β-Qiagen QuantiTect primer assay (QT01048355). Qiagen QuantiTect primers for NLRC4 (QT00264670) and AIM2 (QT00266819) were also used. We used 18S rRNA (PPM57735E; Qiagen) as the housekeeping gene for all the qPCR experiments. No-template controls and dissociation curves were obtained for every experiment to exclude cross-contamination.

Coimmunoprecipitation studies

We treated 5 × 10^6 primary microglia per treatment group with aggregated αSyn or vehicle for 30 min. Cell lysates were prepared in TNE buffer (10 mM Tris-HCl, pH 7.5, 1% Nonidet P-40, 0.15 M NaCl, 1 mM EDTA, and 1:100 protease inhibitor mixture). Pellets were resuspended in TNE buffer and kept on ice for 30 min. The lysates were then centrifuged at 17,400 ×*g* for 35 min at 4°C. The supernatant protein concentration was measured and normalized between samples. Approximately 50 µg protein was used as the input fraction. For immunoprecipitation analysis, 400–500 µg protein per sample in 500 µl TNE buffer was used. We added 5 µg of goat polyclonal TLR2 or CD36 antibody to the lysates before setting them on an orbital shaker overnight at 4°C. The next day, protein G Sepharose beads were added to each sample, and orbital shaking continued overnight at 4°C. Protein G beads were collected by centrifugation at 2,000 ×*g* for 5 min and washed four times with TNE buffer. The bound proteins were eluted by boiling in protein-loading dye for 5 min. Immunoblots were performed on 12% SDS-PAGE gels as described in Immunoblotting. To pull down FLAG-tagged CD36 from transfected HEK cells, anti-FLAG M2 magnetic beads (Sigma-Aldrich) were used.

Casp-1 assays

WT and $Fyn^{-/-}$ microglial cells were plated onto poly-D-lysine (PDL)–coated 96-well plates at 150,000 cells per well. Cells were treated with aggregated αSyn at the prespecified doses. The FLICA dye was added in PBS for 30 min at 37°C. The cells were washed in PBS three times after treatment, and fluorescence was read per the manufacturer's instructions.

Nuclear and cytoplasmic fractionation

Nuclear and cytoplasmic fractions were performed using the NE-PER Kit (Thermo Fisher Scientific) as previously described (Jin et al., 2011a). Briefly, 5 × 10^6 cells were treated with aggregated αSyn for 30 min. CER1 reagent (150–200 µl) was used per sample to extract the cytoplasmic fraction, and 45 µl of NER reagent was used to extract the nuclear fraction.

Nitric oxide detection

Nitric oxide production by primary microglia was measured indirectly by quantification of nitrite in the supernatant using the Griess reagent (Sigma-Aldrich). Microglia were plated in PDL-coated 96-well plates at 10^5 cells/well. Cells were treated with aggregated αSyn for 24 h after priming with LPS for 3 h. After 100 µl of supernatant was collected from each well, an equal volume of the Griess reagent was added. The samples were incubated on a plate shaker at RT for 15 min until a stable color was obtained. The absorbance at 540 nm was measured using a Synergy 2 multimode microplate reader (BioTek Instruments), and the nitrite concentration was determined from a sodium nitrite standard curve.

Multiplex cytokine Luminex immunoassays

Primary microglia obtained from WT, $PKC\delta^{-/-}$, and $Fyn^{-/-}$ mice were seeded in PDL-coated 96-well plates at 10^5 cells/well. After treating the cells with aggregated αSyn for 24 h, 50 µl of supernatant from each well was collected and frozen at −80°C. The levels of cytokines and chemokines in the supernatants were determined using the Luminex bead-based immunoassay platform (Vignali 2000) and prevalidated multiplex kits (Milliplex mouse cytokine panel; EMD Millipore) according to the manufacturer's instructions.

Mouse IL-1β ELISA

The IL-1β duoset ELISA kit (DY401-05; R&D Biosystems) was used to assess microglial IL-1β secretion in Fig. 4 I.

Transfections of primary microglia

The predesigned, on-target plus SMART pool Fyn siRNA (a combination of four siRNAs, LQ-040112-00-0002) and scrambled siRNA (D-001210-03-05) were purchased from Dharmacon. We performed siRNA transfections in primary mouse microglial cells with Lipofectamine 3000 reagent according to the manufacturer's protocol. Briefly, primary microglia were plated at 2 × 10^6 cells/well in 6-well plates one day before transfection. For each well, 300 pmol of Fyn siRNA pool (75 pmol each) or an equal amount of scramble siRNA mixed with 5 µl of Lipofectamine 3000 was added to the cells. Then, 72 h after the initial transfection, cells were treated with aggregated αSyn for 4 h. Lysates prepared in modified RIPA buffer, as mentioned in Immunoblotting, were checked for the expression of pro–IL-1β and Fyn. Transfection of primary microglia with WT Fyn-FLAG and Y417A Fyn-FLAG plasmid constructs was also performed using 5 µl of Lipofectamine 3000, but this was left on for 48 h. FLAG immunoblots were performed to check for successful transfections.

IHC and immunofluorescence studies

IHC was performed on sections from the ventral midbrain and other brain regions of interest as described previously (Jin et al.,

2011b; Ghosh et al., 2013). Briefly, mice were anesthetized with a mixture of 200 mg/kg ketamine and 20 mg/kg xylazine and then perfused transcardially with freshly prepared 4% paraformaldehyde (PFA). Extracted brains were postfixed in 4% PFA for 48 h and 30-µm sections were cut using a freezing microtome (Leica Microsystems). Antigen retrieval was performed in sodium citrate buffer (10 mM, pH 8.5) for 30 min at 90°C. PBS-washed sections were blocked with PBS containing 2% BSA, 0.2% Triton X-100 and 0.05% Tween-20 for 1 h at RT before being incubated with primary antibodies overnight at 4°C and washed seven times in PBS on a Belly Dancer Shaker (SPI supplies). Sections were incubated with Alexa 488, 555, and 633 dye-conjugated secondary antibodies for 75 min at RT and their cell nuclei were stained with Hoechst dye. Sections slide-mounted using Prolong antifade gold mounting medium (Invitrogen) were photomicrographed using a Spot digital camera (Diagnostic Instruments Inc.) coupled to an inverted fluorescence microscope (TE-2000U; Nikon). Immunofluorescence studies in primary microglia were performed according to previously published protocols with some modifications (Gordon et al., 2011). Briefly, cells were plated onto PDL-coated coverslips. After treatments, cells were fixed with 4% PFA, washed in PBS, and incubated in blocking buffer (PBS containing 1.5% BSA, 0.5% Triton X-100, and 0.05% Tween-20) for 1 h at RT. Coverslips were then incubated overnight at 4°C with the respective primary antibodies diluted in PBS containing 1% BSA. Samples were then washed several times in PBS and incubated with Alexa Fluor 488 and Alexa Fluor 555 dye-conjugated secondary antibodies. The nuclei were labeled with Hoechst stain (10 µg/ml), and coverslips were mounted with Fluoromount medium (Sigma-Aldrich) on glass slides for visualization. ASC-CFP fluorescence was imaged by assessing the natural fluorescence using the CFP filter on a Leica DMIRE2 confocal microscope.

Confocal imaging and Z-stack image acquisition and analysis

Confocal imaging was performed at the Iowa State University's Microscopy Facility using the Leica DMIRE2 confocal microscope with the 63× and 40× oil objectives and Leica Confocal Software. One optical series covered 11–13 optical slices of 0.5-µm thickness each. Imaris software was used to analyze Z-stack images. The surface reconstruction wizard in Imaris was used to generate 3D reconstructions of stacks for easier viewing of microglial-dopaminergic contacts. IHC on human sections was performed as described above, but with some modifications. Antigen retrieval was done overnight in sodium citrate buffer (10 mM, pH 8.5) at 4°C before the 90°C step.

MitoROS measurement

MitoROS generation was quantified using the MitoSOX red fluorescent indicator. WT and Fyn$^{-/-}$ microglia were plated onto coverslips at 150,000 cells per well. We added aggregated αSyn and the MitoSOX probe (1 µM) to the cells at the same time. Fluorescence expressed by the generated mitochondrial superoxides was measured hourly for 0–12 h using Cytation 3 Cell Imaging Multi-Mode Reader (BioTek Instruments) as per the manufacturer's instructions.

Mitochondrial visualization

Microglia obtained via the shake-off method were plated onto PDL-coated coverslips. After treatment under various paradigms, 300 µl of 166-nM CMXROS MitoTracker red dye diluted in serum-free DMEM/F12 media was added and incubated at 37°C for 13 min. After incubation, wells were gently washed with PBS three to five times and then fixed in 4% PFA for 30 min. The wells were washed with PBS three times. After this, ICC for Iba-1 was performed as described under IHC and immunofluorescence studies.

Data analysis

Data analysis was performed using Prism 4.0 (GraphPad Software). Data were initially analyzed using one-way ANOVA and Bonferroni's post-test to compare the means of treatment groups. Student's *t* test was used when comparing two groups. Differences of $P < 0.05$ were considered statistically significant. In all figures, error bars represent mean ± SEM. In each figure, asterisks indicate the level of statistical significance: ns, not significant; *, $P \le 0.05$; **, $P \le 0.01$; ***, $P \le 0.001$.

Study approval

Iowa State University's (ISU) laboratory animal facility is fully accredited by the Association for Assessment and Accreditation of Laboratory Animal Care, and all procedures involving animal handling at ISU were approved by the Institutional Animal Care and Use Committee at ISU. All procedures involving animals at the Johns Hopkins University School of Medicine were approved by and conformed to the guidelines of the Institutional Animal Care and Use Committee of Johns Hopkins University.

Human experimental guidelines approval statement

The John Hopkins Medical Institutions' Joint Committee on Clinical Investigations decided that these studies are exempt from Human Subjects Approval because of Federal Register 46.101 Exemption Number 4.

Online supplemental material

Fig. S1 shows our protocol for obtaining and aggregating (human) αSyn. Fig. S2 shows that αSyn can activate the LPS-primed NLRP3 inflammasome in microglia. Fig. S3 shows that Fyn kinase mediates inflammogen-mediated priming of the microglial NLRP3 inflammasome. Fig. S4 demonstrates that CD36 contributes to αSyn-mediated NLRP3 inflammasome priming. Fig. S5 shows diminished microglial NLRP3 induction in Fyn$^{-/-}$ mice following AAV-SYN injection. Table S1 lists details of postmortem PD and control SN brain samples.

Acknowledgments

We would like to thank Dr. Juan C. Troncoso (Department of Pathology, Johns Hopkins University School of Medicine, Baltimore, MD) for providing control and PD human sections. We also thank Gary Zenitsky for assistance in preparing this manuscript.

This study was supported by the National Institutes of Health (grants NS088206, ES026892, and NS100090). The W.E. Lloyd

Endowed Chair and Eminent Scholar in Veterinary Medicine and Armbrust Endowment (to A.G. Kanthasamy) and the Salisbury Endowed Chair (to A. Kanthasamy) are also acknowledged. The Johns Hopkins University Alzheimer's Disease Research Center Grant (National Institutes of Health grant P50 AG05146) and the Institutional Center Core Grant to the Johns Hopkins Multiphoton Imaging Core (National Institutes of Health grant NS050274) are acknowledged. N. Panicker is supported by a postdoctoral fellowship from the Maryland Stem Cell Research Fund (2017-MSCRFF-3838).

A.G. Kanthasamy and V. Anantharam have an equity interest in PK Biosciences Corporation (Ames, IA). The terms of this arrangement have been reviewed and approved by Iowa State University in accordance with its conflict-of-interest policies. The other authors declare no competing financial interests.

Author contributions: N. Panicker, A.G. Kanthasamy, and A. Kanthasamy designed research. N. Panicker, S. Sarkar, D.S. Harischandra, M. Neal, T.-I. Kam, H. Jin, H. Saminathan, M. Langley, A. Charli, M. Samidurai, D. Rokad, and S. Ghaisas performed experiments. N. Panicker and H. Jin analyzed experimental results. V.L. Dawson and T.M. Dawson assisted in conceptualizing αSyn interaction and internalization experiments. O. Pletnikova obtained, sectioned, and provided human control and PD SN sections and assisted in planning SN section staining. N. Panicker, H. Jin, V. Anantharam, A.G. Kanthasamy, and A. Kanthasamy wrote the manuscript, A.G. Kanthasamy and A. Kanthasamy supervised all experiments. V.L. Dawson, T.M. Dawson, A.G. Kanthasamy, A. Kanthasamy, and N. Panicker secured funding.

Submitted: 27 November 2018
Revised: 14 February 2019
Accepted: 22 March 2019

References

Allen Reish, H.E., and D.G. Standaert. 2015. Role of α-synuclein in inducing innate and adaptive immunity in Parkinson disease. *J. Parkinsons Dis.* 5: 1–19.

Appel-Cresswell, S., C. Vilarino-Guell, M. Encarnacion, H. Sherman, I. Yu, B. Shah, D. Weir, C. Thompson, C. Szu-Tu, J. Trinh, et al 2013. Alpha-synuclein p.H50Q, a novel pathogenic mutation for Parkinson's disease. *Mov. Disord.* 28:811–813. https://doi.org/10.1002/mds.25421

Baroja-Mazo, A., F. Martín-Sánchez, A.I. Gomez, C.M. Martínez, J. Amores-Iniesta, V. Compan, M. Barberà-Cremades, J. Yagüe, E. Ruiz-Ortiz, J. Antón, et al 2014. The NLRP3 inflammasome is released as a particulate danger signal that amplifies the inflammatory response. *Nat. Immunol.* 15:738–748. https://doi.org/10.1038/ni.2919

Block, M.L., L. Zecca, and J.S. Hong. 2007. Microglia-mediated neurotoxicity: uncovering the molecular mechanisms. *Nat. Rev. Neurosci.* 8:57–69. https://doi.org/10.1038/nrn2038

Boza-Serrano, A., J.F. Reyes, N.L. Rey, H. Leffler, L. Bousset, U. Nilsson, P. Brundin, J.L. Venero, M.A. Burguillos, and T. Deierborg. 2014. The role of Galectin-3 in α-synuclein-induced microglial activation. *Acta Neuropathol. Commun.* 2:156.

Cao, S., D.G. Standaert, and A.S. Harms. 2012. The gamma chain subunit of Fc receptors is required for alpha-synuclein-induced pro-inflammatory signaling in microglia. *J. Neuroinflammation.* 9:259. https://doi.org/10.1186/1742-2094-9-259

Chen, K., M. Febbraio, W. Li, and R.L. Silverstein. 2008. A specific CD36-dependent signaling pathway is required for platelet activation by oxidized low-density lipoprotein. *Circ. Res.* 102:1512–1519. https://doi.org/10.1161/CIRCRESAHA.108.172064

Codolo, G., N. Plotegher, T. Pozzobon, M. Brucale, I. Tessari, L. Bubacco, and M. de Bernard. 2013. Triggering of inflammasome by aggregated α-synuclein, an inflammatory response in synucleinopathies. *PLoS One.* 8:e55375. https://doi.org/10.1371/journal.pone.0055375

Coll, R.C., A.A. Robertson, J.J. Chae, S.C. Higgins, R. Muñoz-Planillo, M.C. Inserra, I. Vetter, L.S. Dungan, B.G. Monks, A. Stutz, et al 2015. A small-molecule inhibitor of the NLRP3 inflammasome for the treatment of inflammatory diseases. *Nat. Med.* 21:248–255. https://doi.org/10.1038/nm.3806

Daniele, S.G., D. Béraud, C. Davenport, K. Cheng, H. Yin, and K.A. Maguire-Zeiss. 2015. Activation of MyD88-dependent TLR1/2 signaling by misfolded α-synuclein, a protein linked to neurodegenerative disorders. *Sci. Signal.* 8:ra45. https://doi.org/10.1126/scisignal.2005965

Devi, L., V. Raghavendran, B.M. Prabhu, N.G. Avadhani, and H.K. Anandatheerthavarada. 2008. Mitochondrial import and accumulation of alpha-synuclein impair complex I in human dopaminergic neuronal cultures and Parkinson disease brain. *J. Biol. Chem.* 283:9089–9100. https://doi.org/10.1074/jbc.M710012200

Dey, N., H.E. Crosswell, P. De, R. Parsons, Q. Peng, J.D. Su, and D.L. Durden. 2008. The protein phosphatase activity of PTEN regulates SRC family kinases and controls glioma migration. *Cancer Res.* 68:1862–1871. https://doi.org/10.1158/0008-5472.CAN-07-1182

Duewell, P., H. Kono, K.J. Rayner, C.M. Sirois, G. Vladimer, F.G. Bauernfeind, G.S. Abela, L. Franchi, G. Nuñez, M. Schnurr, et al 2010. NLRP3 inflammasomes are required for atherogenesis and activated by cholesterol crystals. *Nature.* 464:1357–1361. https://doi.org/10.1038/nature08938

Fellner, L., R. Irschick, K. Schanda, M. Reindl, L. Klimaschewski, W. Poewe, G.K. Wenning, and N. Stefanova. 2013. Toll-like receptor 4 is required for α-synuclein dependent activation of microglia and astroglia. *Glia.* 61: 349–360. https://doi.org/10.1002/glia.22437

Finberg, R.W., C. Yim, J. Yan, L.C. Cao, L. Mandell, and E.A. Kurt-Jones. 2012. Phosphorylated Toll-Like Receptor 2 Interacts with Fyn and Cross-Talks with the Phosphorylation-Independent TLR2-Signaling Pathway. *Open Immunol. J.* 5:36–45. https://doi.org/10.2174/1874226201205010036

Freeman, L., H. Guo, C.N. David, W.J. Brickey, S. Jha, and J.P. Ting. 2017. NLR members NLRC4 and NLRP3 mediate sterile inflammasome activation in microglia and astrocytes. *J. Exp. Med.* 214:1351–1370. https://doi.org/10.1084/jem.20150237

Ghosh, A., H. Saminathan, A. Kanthasamy, V. Anantharam, H. Jin, G. Sondarva, D.S. Harischandra, Z. Qian, A. Rana, and A.G. Kanthasamy. 2013. The peptidyl-prolyl isomerase Pin1 up-regulation and proapoptotic function in dopaminergic neurons: relevance to the pathogenesis of Parkinson disease. *J. Biol. Chem.* 288:21955–21971. https://doi.org/10.1074/jbc.M112.444224

Glass, C.K., K. Saijo, B. Winner, M.C. Marchetto, and F.H. Gage. 2010. Mechanisms underlying inflammation in neurodegeneration. *Cell.* 140: 918–934. https://doi.org/10.1016/j.cell.2010.02.016

Gombash, S.E., F.P. Manfredsson, C.J. Kemp, N.C. Kuhn, S.M. Fleming, A.E. Egan, L.M. Grant, M.R. Ciucci, J.P. MacKeigan, and C.E. Sortwell. 2013. Morphological and behavioral impact of AAV2/5-mediated overexpression of human wildtype alpha-synuclein in the rat nigrostriatal system. *PLoS One.* 8:e81426. https://doi.org/10.1371/journal.pone.0081426

Gomez, G., C. Gonzalez-Espinosa, S. Odom, G. Baez, M.E. Cid, J.J. Ryan, and J. Rivera. 2005. Impaired FcepsilonRI-dependent gene expression and defective eicosanoid and cytokine production as a consequence of Fyn deficiency in mast cells. *J. Immunol.* 175:7602–7610. https://doi.org/10.4049/jimmunol.175.11.7602

Gordon, R., C.E. Hogan, M.L. Neal, V. Anantharam, A.G. Kanthasamy, and A. Kanthasamy. 2011. A simple magnetic separation method for high-yield isolation of pure primary microglia. *J. Neurosci. Methods.* 194:287–296. https://doi.org/10.1016/j.jneumeth.2010.11.001

Gordon, R., E.A. Albornoz, D.C. Christie, M.R. Langley, V. Kumar, S. Mantovani, A.A.B. Robertson, M.S. Butler, D.B. Rowe, L.A. O'Neill, et al 2018. Inflammasome inhibition prevents α-synuclein pathology and dopaminergic neurodegeneration in mice. *Sci. Transl. Med.* 10:eaah4066. https://doi.org/10.1126/scitranslmed.aah4066

Grassi, D., S. Howard, M. Zhou, N. Diaz-Perez, N.T. Urban, D. Guerrero-Given, N. Kamasawa, L.A. Volpicelli-Daley, P. LoGrasso, and C.I. Lasmézas. 2018. Identification of a highly neurotoxic α-synuclein species inducing mitochondrial damage and mitophagy in Parkinson's disease. *Proc. Natl. Acad. Sci. USA.* 115:E2634–E2643. https://doi.org/10.1073/pnas.1713849115

Gustin, A., M. Kirchmeyer, E. Koncina, P. Felten, S. Losciuto, T. Heurtaux, A. Tardivel, P. Heuschling, and C. Dostert. 2015. NLRP3 Inflammasome Is

Expressed and Functional in Mouse Brain Microglia but Not in Astrocytes. *PLoS One.* 10:e0130624. https://doi.org/10.1371/journal.pone.0130624

Gustot, A., J.I. Gallea, R. Sarroukh, M.S. Celej, J.M. Ruysschaert, and V. Raussens. 2015. Amyloid fibrils are the molecular trigger of inflammation in Parkinson's disease. *Biochem. J.* 471:323–333. https://doi.org/10.1042/BJ20150617

Hafner-Bratkovič, I., M. Benčina, K.A. Fitzgerald, D. Golenbock, and R. Jerala. 2012. NLRP3 inflammasome activation in macrophage cell lines by prion protein fibrils as the source of IL-1β and neuronal toxicity. *Cell. Mol. Life Sci.* 69:4215–4228. https://doi.org/10.1007/s00018-012-1140-0

Halle, A., V. Hornung, G.C. Petzold, C.R. Stewart, B.G. Monks, T. Reinheckel, K.A. Fitzgerald, E. Latz, K.J. Moore, and D.T. Golenbock. 2008. The NALP3 inflammasome is involved in the innate immune response to amyloid-beta. *Nat. Immunol.* 9:857–865. https://doi.org/10.1038/ni.1636

Hayden, M.S., and S. Ghosh. 2004. Signaling to NF-kappaB. *Genes Dev.* 18:2195–2224. https://doi.org/10.1101/gad.1228704

Heneka, M.T., M.P. Kummer, A. Stutz, A. Delekate, S. Schwartz, A. Vieira-Saecker, A. Griep, D. Axt, A. Remus, T.C. Tzeng, et al 2013. NLRP3 is activated in Alzheimer's disease and contributes to pathology in APP/PS1 mice. *Nature.* 493:674–678. https://doi.org/10.1038/nature11729

Imamura, K., N. Hishikawa, M. Sawada, T. Nagatsu, M. Yoshida, and Y. Hashizume. 2003. Distribution of major histocompatibility complex class II-positive microglia and cytokine profile of Parkinson's disease brains. *Acta Neuropathol.* 106:518–526. https://doi.org/10.1007/s00401-003-0766-2

Jin, H., A. Kanthasamy, V. Anantharam, A. Rana, and A.G. Kanthasamy. 2011a. Transcriptional regulation of pro-apoptotic protein kinase Cdelta: implications for oxidative stress-induced neuronal cell death. *J. Biol. Chem.* 286:19840–19859. https://doi.org/10.1074/jbc.M110.203687

Jin, H., A. Kanthasamy, A. Ghosh, Y. Yang, V. Anantharam, and A.G. Kanthasamy. 2011b. α-Synuclein negatively regulates protein kinase Cδ expression to suppress apoptosis in dopaminergic neurons by reducing p300 histone acetyltransferase activity. *J. Neurosci.* 31:2035–2051. https://doi.org/10.1523/JNEUROSCI.5634-10.2011

Kaspar, J.W., and A.K. Jaiswal. 2011. Tyrosine phosphorylation controls nuclear export of Fyn, allowing Nrf2 activation of cytoprotective gene expression. *FASEB J.* 25:1076–1087. https://doi.org/10.1096/fj.10-171553

Kaufman, A.C., S.V. Salazar, L.T. Haas, J. Yang, M.A. Kostylev, A.T. Jeng, S.A. Robinson, E.C. Gunther, C.H. van Dyck, H.B. Nygaard, and S.M. Strittmatter. 2015. Fyn inhibition rescues established memory and synapse loss in Alzheimer mice. *Ann. Neurol.* 77:953–971. https://doi.org/10.1002/ana.24394

Kayagaki, N., S. Warming, M. Lamkanfi, L. Vande Walle, S. Louie, J. Dong, K. Newton, Y. Qu, J. Liu, S. Heldens, et al 2011. Non-canonical inflammasome activation targets caspase-11. *Nature.* 479:117–121. https://doi.org/10.1038/nature10558

Kim, C., D.H. Ho, J.E. Suk, S. You, S. Michael, J. Kang, S. Joong Lee, E. Masliah, D. Hwang, H.J. Lee, and S.J. Lee. 2013. Neuron-released oligomeric α-synuclein is an endogenous agonist of TLR2 for paracrine activation of microglia. *Nat. Commun.* 4:1562. https://doi.org/10.1038/ncomms2534

Krüger, R., W. Kuhn, T. Müller, D. Woitalla, M. Graeber, S. Kösel, H. Przuntek, J.T. Epplen, L. Schöls, and O. Riess. 1998. Ala30Pro mutation in the gene encoding alpha-synuclein in Parkinson's disease. *Nat. Genet.* 18:106–108. https://doi.org/10.1038/ng0298-106

Kuri, P., N.L. Schieber, T. Thumberger, J. Wittbrodt, Y. Schwab, and M. Leptin. 2017. Dynamics of in vivo ASC speck formation. *J. Cell Biol.* 216:2891–2909. https://doi.org/10.1083/JCB.20170310308302017c

Lambert, M.P., A.K. Barlow, B.A. Chromy, C. Edwards, R. Freed, M. Liosatos, T.E. Morgan, I. Rozovsky, B. Trommer, K.L. Viola, et al 1998. Diffusible, nonfibrillar ligands derived from Abeta1-42 are potent central nervous system neurotoxins. *Proc. Natl. Acad. Sci. USA.* 95:6448–6453. https://doi.org/10.1073/pnas.95.11.6448

Lamkanfi, M., and V.M. Dixit. 2014. Mechanisms and functions of inflammasomes. *Cell.* 157:1013–1022. https://doi.org/10.1016/j.cell.2014.04.007

Latz, E., T.S. Xiao, and A. Stutz. 2013. Activation and regulation of the inflammasomes. *Nat. Rev. Immunol.* 13:397–411. https://doi.org/10.1038/nri3452

Lee, E.J., M.S. Woo, P.G. Moon, M.C. Baek, I.Y. Choi, W.K. Kim, E. Junn, and H.S. Kim. 2010. Alpha-synuclein activates microglia by inducing the expressions of matrix metalloproteinases and the subsequent activation of protease-activated receptor-1. *J. Immunol.* 185:615–623. https://doi.org/10.4049/jimmunol.0903480

Lee, H.M., J.J. Kim, H.J. Kim, M. Shong, B.J. Ku, and E.K. Jo. 2013. Upregulated NLRP3 inflammasome activation in patients with type 2 diabetes. *Diabetes.* 62:194–204. https://doi.org/10.2337/db12-0420

Lesage, S., M. Anheim, F. Letournel, L. Bousset, A. Honoré, N. Rozas, L. Pieri, K. Madiona, A. Dürr, R. Melki, et al; French Parkinson's Disease Genetics Study Group. 2013. G51D α-synuclein mutation causes a novel parkinsonian-pyramidal syndrome. *Ann. Neurol.* 73:459–471. https://doi.org/10.1002/ana.23894

Luk, K.C., V. Kehm, J. Carroll, B. Zhang, P. O'Brien, J.Q. Trojanowski, and V.M. Lee. 2012. Pathological α-synuclein transmission initiates Parkinson-like neurodegeneration in nontransgenic mice. *Science.* 338:949–953. https://doi.org/10.1126/science.1227157

Lukens, J.R., J.M. Gross, C. Calabrese, Y. Iwakura, M. Lamkanfi, P. Vogel, and T.D. Kanneganti. 2014. Critical role for inflammasome-independent IL-1β production in osteomyelitis. *Proc. Natl. Acad. Sci. USA.* 111:1066–1071. https://doi.org/10.1073/pnas.1318688111

Luth, E.S., I.G. Stavrovskaya, T. Bartels, B.S. Kristal, and D.J. Selkoe. 2014. Soluble, prefibrillar α-synuclein oligomers promote complex I-dependent, Ca2+-induced mitochondrial dysfunction. *J. Biol. Chem.* 289:21490–21507. https://doi.org/10.1074/jbc.M113.545749

Mao, X., M.T. Ou, S.S. Karuppagounder, T.I. Kam, X. Yin, Y. Xiong, P. Ge, G.E. Umanah, S. Brahmachari, J.H. Shin, et al 2016. Pathological α-synuclein transmission initiated by binding lymphocyte-activation gene 3. *Science.* 353:aah3374. https://doi.org/10.1126/science.aah3374

Mayer-Barber, K.D., D.L. Barber, K. Shenderov, S.D. White, M.S. Wilson, A. Cheever, D. Kugler, S. Hieny, P. Caspar, G. Núñez, et al 2010. Caspase-1 independent IL-1beta production is critical for host resistance to mycobacterium tuberculosis and does not require TLR signaling in vivo. *J. Immunol.* 184:3326–3330. https://doi.org/10.4049/jimmunol.0904189

Mogi, M., M. Harada, H. Narabayashi, H. Inagaki, M. Minami, and T. Nagatsu. 1996. Interleukin (IL)-1 beta, IL-2, IL-4, IL-6 and transforming growth factor-alpha levels are elevated in ventricular cerebrospinal fluid in juvenile parkinsonism and Parkinson's disease. *Neurosci. Lett.* 211:13–16. https://doi.org/10.1016/0304-3940(96)12706-3

Mogi, M., A. Togari, T. Kondo, Y. Mizuno, O. Komure, S. Kuno, H. Ichinose, and T. Nagatsu. 2000. Caspase activities and tumor necrosis factor receptor R1 (p55) level are elevated in the substantia nigra from parkinsonian brain. *J. Neural Transm. (Vienna).* 107:335–341. https://doi.org/10.1007/s007020050028

Moore, K.J., J. El Khoury, L.A. Medeiros, K. Terada, C. Geula, A.D. Luster, and M.W. Freeman. 2002. A CD36-initiated signaling cascade mediates inflammatory effects of beta-amyloid. *J. Biol. Chem.* 277:47373–47379. https://doi.org/10.1074/jbc.M208788200

Nalls, M.A., C. Blauwendraat, C.L. Vallerga, K. Heilbron, S. Bandres-Ciga, D. Chang, M. Tan, D.A. Kia, A.J. Noyce, A. Xue, et al 2018. Parkinson's disease genetics: identifying novel risk loci, providing causal insights and improving estimates of heritable risk. *bioRxiv.* doi:10.1101/388165 (Preprint posted August 9, 2018).

Netea, M.G., C.A. Nold-Petry, M.F. Nold, L.A. Joosten, B. Opitz, J.H. van der Meer, F.L. van de Veerdonk, G. Ferwerda, B. Heinhuis, I. Devesa, et al 2009. Differential requirement for the activation of the inflammasome for processing and release of IL-1beta in monocytes and macrophages. *Blood.* 113:2324–2335. https://doi.org/10.1182/blood-2008-03-146720

Palacios, E.H., and A. Weiss. 2004. Function of the Src-family kinases, Lck and Fyn, in T-cell development and activation. *Oncogene.* 23:7990–8000. https://doi.org/10.1038/sj.onc.1208074

Panicker, N., H. Saminathan, H. Jin, M. Neal, D.S. Harischandra, R. Gordon, K. Kanthasamy, V. Lawana, S. Sarkar, J. Luo, et al 2015. Fyn Kinase Regulates Microglial Neuroinflammatory Responses in Cell Culture and Animal Models of Parkinson's Disease. *J. Neurosci.* 35:10058–10077. https://doi.org/10.1523/JNEUROSCI.0302-15.2015

Pasanen, P., L. Myllykangas, M. Siitonen, A. Raunio, S. Kaakkola, J. Lyytinen, P.J. Tienari, M. Pöyhönen, and A. Paetau. 2014. Novel α-synuclein mutation A53E associated with atypical multiple system atrophy and Parkinson's disease-type pathology. *Neurobiol. Aging.* 35:2180.e1–2180.e5. https://doi.org/10.1016/j.neurobiolaging.2014.03.024

Peng, C., R.J. Gathagan, D.J. Covell, C. Medellin, A. Stieber, J.L. Robinson, B. Zhang, R.M. Pitkin, M.F. Olufemi, K.C. Luk, et al 2018. Cellular milieu imparts distinct pathological α-synuclein strains in α-synucleinopathies. *Nature.* 557:558–563. https://doi.org/10.1038/s41586-018-0104-4

Polymeropoulos, M.H., C. Lavedan, E. Leroy, S.E. Ide, A. Dehejia, A. Dutra, B. Pike, H. Root, J. Rubenstein, R. Boyer, et al 1997. Mutation in the alpha-synuclein gene identified in families with Parkinson's disease. *Science.* 276:2045–2047. https://doi.org/10.1126/science.276.5321.2045

Qu, Y., S. Misaghi, A. Izrael-Tomasevic, K. Newton, L.L. Gilmour, M. Lamkanfi, S. Louie, N. Kayagaki, J. Liu, L. Kömüves, et al 2012. Phosphorylation of NLRC4 is critical for inflammasome activation. *Nature.* 490: 539–542. https://doi.org/10.1038/nature11429

Reeve, A.K., M.H. Ludtmann, P.R. Angelova, E.M. Simcox, M.H. Horrocks, D. Klenerman, S. Gandhi, D.M. Turnbull, and A.Y. Abramov. 2015. Aggregated α-synuclein and complex I deficiency: exploration of their relationship in differentiated neurons. *Cell Death Dis.* 6:e1820. https://doi.org/10.1038/cddis.2015.166

Sarkar, S., E. Malovic, D.S. Harishchandra, S. Ghaisas, N. Panicker, A. Charli, B.N. Palanisamy, D. Rokad, H. Jin, V. Anantharam, et al 2017. Mitochondrial impairment in microglia amplifies NLRP3 inflammasome proinflammatory signaling in cell culture and animal models of Parkinson's disease. *NPJ Parkinsons Dis.* 3:30. https://doi.org/10.1038/s41531-017-0032-2

Sarkar, S., E. Malovic, D. Sarda, V. Lawana, D. Rokad, H. Jin, V. Anantharam, A. Kanthasamy, and A.G. Kanthasamy. 2018. Characterization and comparative analysis of a new mouse microglial cell model for studying neuroinflammatory mechanisms during neurotoxic insults. *Neurotoxicology.* 67:129–140. https://doi.org/10.1016/j.neuro.2018.05.002

Seo, J., E.W. Ottesen, and R.N. Singh. 2014. Antisense methods to modulate pre-mRNA splicing. *Methods Mol. Biol.* 1126:271–283. https://doi.org/10.1007/978-1-62703-980-2_20

Sheedy, F.J., A. Grebe, K.J. Rayner, P. Kalantari, B. Ramkhelawon, S.B. Carpenter, C.E. Becker, H.N. Ediriweera, A.E. Mullick, D.T. Golenbock, et al 2013. CD36 coordinates NLRP3 inflammasome activation by facilitating intracellular nucleation of soluble ligands into particulate ligands in sterile inflammation. *Nat. Immunol.* 14:812–820. https://doi.org/10.1038/ni.2639

Sperber, B.R., E.A. Boyle-Walsh, M.J. Engleka, P. Gadue, A.C. Peterson, P.L. Stein, S.S. Scherer, and F.A. McMorris. 2001. A unique role for Fyn in CNS myelination. *J. Neurosci.* 21:2039–2047. https://doi.org/10.1523/JNEUROSCI.21-06-02039.2001

Stuart, L.M., S.A. Bell, C.R. Stewart, J.M. Silver, J. Richard, J.L. Goss, A.A. Tseng, A. Zhang, J.B. El Khoury, and K.J. Moore. 2007. CD36 signals to the actin cytoskeleton and regulates microglial migration via a p130Cas complex. *J. Biol. Chem.* 282:27392–27401. https://doi.org/10.1074/jbc.M702887200

Stutz, A., G.L. Horvath, B.G. Monks, and E. Latz. 2013. ASC speck formation as a readout for inflammasome activation. *Methods Mol. Biol.* 1040:91–101. https://doi.org/10.1007/978-1-62703-523-1_8

Su, X., K.A. Maguire-Zeiss, R. Giuliano, L. Prifti, K. Venkatesh, and H.J. Federoff. 2008. Synuclein activates microglia in a model of Parkinson's disease. *Neurobiol. Aging.* 29:1690–1701. https://doi.org/10.1016/j.neurobiolaging.2007.04.006

Tansey, M.G., and M.S. Goldberg. 2010. Neuroinflammation in Parkinson's disease: its role in neuronal death and implications for therapeutic intervention. *Neurobiol. Dis.* 37:510–518. https://doi.org/10.1016/j.nbd.2009.11.004

Tschopp, J., and K. Schroder. 2010. NLRP3 inflammasome activation: The convergence of multiple signalling pathways on ROS production? *Nat. Rev. Immunol.* 10:210–215. https://doi.org/10.1038/nri2725

Tu, P.H., J.E. Galvin, M. Baba, B. Giasson, T. Tomita, S. Leight, S. Nakajo, T. Iwatsubo, J.Q. Trojanowski, and V.M. Lee. 1998. Glial cytoplasmic inclusions in white matter oligodendrocytes of multiple system atrophy brains contain insoluble alpha-synuclein. *Ann. Neurol.* 44:415–422. https://doi.org/10.1002/ana.410440324

Venegas, C., S. Kumar, B.S. Franklin, T. Dierkes, R. Brinkschulte, D. Tejera, A. Vieira-Saecker, S. Schwartz, F. Santarelli, M.P. Kummer, et al 2017. Microglia-derived ASC specks cross-seed amyloid-β in Alzheimer's disease. *Nature.* 552:355–361. https://doi.org/10.1038/nature25158

Walsh, J.G., D.A. Muruve, and C. Power. 2014. Inflammasomes in the CNS. *Nat. Rev. Neurosci.* 15:84–97. https://doi.org/10.1038/nrn3638

Zarranz, J.J., J. Alegre, J.C. Gómez-Esteban, E. Lezcano, R. Ros, I. Ampuero, L. Vidal, J. Hoenicka, O. Rodriguez, B. Atarés, et al 2004. The new mutation, E46K, of alpha-synuclein causes Parkinson and Lewy body dementia. *Ann. Neurol.* 55:164–173. https://doi.org/10.1002/ana.10795

Zhang, W., T. Wang, Z. Pei, D.S. Miller, X. Wu, M.L. Block, B. Wilson, W. Zhang, Y. Zhou, J.S. Hong, and J. Zhang. 2005. Aggregated alpha-synuclein activates microglia: a process leading to disease progression in Parkinson's disease. *FASEB J.* 19:533–542. https://doi.org/10.1096/fj.04-2751com

Zhou, R., A.S. Yazdi, P. Menu, and J. Tschopp. 2011. A role for mitochondria in NLRP3 inflammasome activation. *Nature.* 469:221–225. https://doi.org/10.1038/nature09663